Table 2 Parameters for trabecular bone were measured below the growth plate at the proximal metaphysis of the tibia in Toluidine-Blue and calcein double-labeled sections

	WT	Ad-Tg Line 11	Ad-Tg Line 13
BV/TV (%)	12.6 ± 2.7	16.1 ± 2.5*	17.3 ± 1.7**
Tb.N (/mm)	3.3 ± 0.3	3.9 ± 0.4*	3.9 ± 0.5*
OS/BS (%)	7.1 ± 4.1	17.7 ± 4.9**	15.4 ± 3.5*
O.Th (μm)	2.8 ± 0.2	3.3 ± 0.1**	2.8 ± 0.2
Ob.S/BS (%)	3.3 ± 2.8	7.4 ± 2.2*	9.3 ± 5.4**
N.Oc/B.Pm (/100 mm)	123.7 ± 41.1	112.2 ± 41.8	132.1 ± 60.7
Oc.S/BS (%)	1.0 ± 0.5	1.1 ± 0.7	1.4 ± 0.5
ES/BS (%)	2.7 ± 1.4	3.3 ± 1.5	4.4 ± 1.1
MAR (μm/day)	1.4 ± 0.2	1.7 ± 0.1**	1.6 ± 0.1*
MS/BS (%)	19.1 ± 3.2	33.1 ± 2.9**	26.8 ± 5.2*
BFR/BS (mm^3/mm^2/year)	0.09 ± 0.02	0.18 ± 0.03**	0.14 ± 0.03**
dLS/BS (%)	7.0 ± 1.0	20.7 ± 2.0**	14.6 ± 4.2**

BV/TV, bone volume/total tissue volume; Tb. N, trabecular number; OS/BS, osteoid surface/bone surface; O.Th, osteoid thickness; Ob.S/BS, osteoblast surface/bone surface; N.Oc/B.Pm, osteoclast number/bone perimeter; Oc.S/BS, osteoclast surface/bone surface; ES/BS, eroded surface/bone surface; MAR, mineral apposition rate; MS/BS (mineralization ratio), mineralizing surface/bone surface; BFR/BS, bone formation rate/bone surface; dLS/BS, double labeled surface/bone surface. Data are expressed as means ± S.D. of 8 bones/group. *P < 0.05, **P < 0.01, significantly different from WT mice.

Another study has demonstrated that female Ad-Tg mice had a significantly lower bone mineral content at 8 and 16 weeks of age, and that the femur neck peak load was significantly lower in 8-week-old Ad-Tg mice of both genders, in comparison with controls [21]. They concluded that circulating adiponectin is a negative regulator of bone mineral and bone strength in mice. For their study, they used transgenic mice expressing a dominant mutation in the collagenous domain of adiponectin, resulting in an increased level of adiponectin complexes including full-length adiponectin; there was also a sexual dimorphism in that females had significantly higher circulating levels than males [21].

Two groups have previously reported the skeletal changes in Ad KO mice. Shinoda et al. found no effect on bone phenotype in Ad-knockout mice at 8 weeks of age [10]. Williams et al. reported increases in the number of trabeculae and bone volume of the proximal tibia at 14 week of age, but non-significant trends at 8 and 22 weeks, in Ad-knockout mice [24]. Interpreted broadly, these studies gave similar results: wild-type and Ad-knockout mice are similar in early life, but differences emerge in adulthood. Most investigators have consistently demonstrated that Ad-knockout mice have either spontaneous or diet-induced insulin resistance, with hyperinsulinemia [25,26]. Thus, insulin resistance is one potential explanation for the increased bone mass in Ad-knockout mice.

The present study utilized 12-week-old male mice overexpressing human full-length adiponectin specifically in the liver and focused on the endocrine effects of this molecule on bone, since human adiponectin is biologically active in mice [14,27]. A noteworthy finding was that circulating human full-length adiponectin increased bone mass and BMD in Ad-Tg mice by promoting osteoblast formation while osteoclast number remained normal. To our knowledge, similar findings have not been reported previously.

According to the recent in vitro studies [8,10], we have demonstrated that circulating human full-length adiponectin increased bone formation in mice. In our previous study, hyperadiponectinemia in the transgenic mice resulted in suppression of fat accumulation and prevention of premature death by a high-calorie diet, leading to an increase of insulin sensitivity [14]. It is therefore considered that the increased osteoblastgenesis may have resulted from the anabolic effects of insulin on bone. In addition, an increase in osteoblast number could well be the result of decreased oxidative stress that attenuates the apoptosis of pre-existing osteoblasts [28]. The latter interpretation is consistent with the evidence discussed previously regarding the phenotype of age-related/Ad KO mice with altered adiponectin expression.

In the present study, circulating human full-length adiponectin did not affect the number of osteoclasts. There was no significant difference in serum RANKL/OPG levels between Ad-Tg mice and their WT littermates. Bone histomorphometric and immunohistochemical analysis consistently demonstrated normal osteoclast function in Ad-Tg mice. As mentioned above, increased insulin sensitivity was thought to be an important factor for skeletal phenotype in our transgenic mice. The major substrates of insulin are known to be closely related insulin receptor substrate-1 and -2: IRS-1 and -2 [29]. Osteoclastic cells showed IRS-2 expression, but not IRS-1 expression [30]. Intrinsic IRS-2 in osteoclastic cells was not important for their differentiation, function, or survival despite the fact that IRS-2 and receptors of insulin are expressed in these cells [31,32]. Thus, these observations may explain why the circulating human full-length adiponectin did not influence the number of osteoclast in the transgenic mice.

Conclusions

We have demonstrated that elevation of the circulating adiponectin level increases bone mass by activating bone formation while normal osteoclast function is retained. Our study confirms that hyperadiponectinemia positively regulates osteogenesis, thus enhancing bone formation.

Abbreviations

Ad-Tg mice: Adiponectin Transgenic mice; WT: Wild Type; BMD: Bone Mineral Density; BMC: Bone Mineral Content; OC: Osteocalcin; IRS: Insulin Receptor Substrate

Acknowledgements
We thank Ms. H. Wakita, Mr. K. Yoshida, and T. Yokoyama, PhD. for providing expert technical assistance.

Author details
[1]Department of Orthopedic Surgery, Kurume University, 67 Asahi-machi, Kurume, Fukuoka 830-0011, Japan. [2]Department of Orthopedic Surgery, Kurume University Medical Center, 155 Kokubu-machi, Kurume, Fukuoka 839-0863, Japan. [3]Division of Endocrinology and Metabolism, Department of Medicine, Kurume University, 67 Asahi-machi, Kurume, Fukuoka 830-0011, Japan.

Authors' contributions
YM, MG and NF designed the study and drafted the manuscript. YM, NF, IS, SO, XY, TH, NW, AM, TY and SY performed the experimental work and the statistical analysis. KY and KN participated in study design. All authors have read and approved the final manuscript.

Competing interests
The authors declare that they have no competing interests.

Received: 13 June 2010 Accepted: 17 January 2011
Published: 17 January 2011

References

1. Smith DM, Khairi MR, Johnston CC Jr: **The loss of bone mineral with aging and its relationship to risk of fracture.** *J Clin Invest* 1975, **56**:311-318.
2. Riggs BL, Melton LJ III: **Involutional osteoporosis.** *N Engl J Med* 1986, **314**:1676-1686.
3. Maeda K, Okubo K, Shimomura I, Mizuno K, Matsuzawa Y, Matsubara K: **Analysis of an expression profile of genes in the human adipose tissue.** *Gene* 1997, **190**:227-235.
4. Kadowaki T, Yamauchi T: **Adiponectin and adiponectin receptors.** *Endocr Rev* 2005, **26**:439-451.
5. Arita Y, Kihara S, Ouchi N, Takahashi M, Maeda K, Miyagawa J, *et al*: **Paradoxical decrease of an adipose-specific protein, adiponectin, in obesity.** *Biochem Biophys Res Commun* 1999, **257**:79-83.
6. Combs TP, Berg AH, Obici S, Scherer PE, Rossetti L: **Endogenous glucose production is inhibited by the adipose-derived protein Acrp30.** *J Clin Invest* 2001, **108**:1875-1881.
7. Berg AH, Combs TP, Du X, Brownlee M, Scherer PE: **The adipocyte-secreted protein Acrp30 enhances hepatic insulin action.** *Nat Med* 2001, **7**:947-953.
8. Oshima K, Nampei A, Matsuda M, Iwaki M, Fukuhara A, Hashimoto J, *et al*: **Adiponectin increases bone mass by suppressing osteoclast and activating osteoblast.** *Biochem Biophys Res Commun* 2005, **331**:520-526.
9. Luo XH, Guo LJ, Yuan LQ, Xie H, Zhou HD, Wu XP, *et al*: **Adiponectin stimulates human osteoblasts proliferation and differentiation via the MAPK signaling pathway.** *Exp Cell Res* 2005, **309**:99-109.
10. Shinoda Y, Yamaguchi M, Ogata N, Akune T, Kubota N, Yamauchi T, *et al*: **Regulation of bone formation by adiponectin through autocrine/paracrine and endocrine pathways.** *J Cell Biochem* 2006, **99**:196-208.
11. Tamura T, Yoneda M, Yamane K, Nakanishi S, Nakashima R, Okubo M, *et al*: **Serum leptin and adiponectin are positively associated with bone mineral density at the distal radius in patients with type 2 diabetes mellitus.** *Metabolism* 2007, **56**:623-628.
12. Luo XH, Guo LJ, Xie H, Yuan LQ, Wu XP, Zhou HD, *et al*: **Adiponectin stimulates RANKL and inhibits OPG expression in human osteoblasts through the MAPK signaling pathway.** *J Bone Miner Res* 2006, **21**:1648-1656.
13. Peng XD, Xie H, Zhao Q, Wu XP, Sun ZQ, Liao EY: **Relationships between serum adiponectin, leptin, resistin, visfatin levels and bone mineral density, and bone biochemical markers in Chinese men.** *Clin Chim Acta* 2008, **387**:31-35.
14. Otabe S, Yuan X, Fukutani T, Wada N, Hashinaga T, Nakayama H, *et al*: **Overexpression of human adiponectin in transgenic mice results in suppression of fat accumulation and prevention of premature death by high-calorie diet.** *Am J Physiol Endocrinol Metab* 2007, **293**:E210-218.
15. Parfitt AM, Drezner MK, Glorieux FH, Kanis JA, Malluche H, Meunier PJ, *et al*: **Bone histomorphometry: standardization of nomenclature, symbols, and units. Report of the ASBMR Histomorphometry Nomenclature Committee.** *J Bone Miner Res* 1987, **2**:595-610.
16. Galli M, Nuti R, Franci B, Righi G, Martorelli MT, Turchetti V, *et al*: **Serum osteocalcin radioimmunoassay in bone diseases.** *Ric Clin Lab* 1985, **15**:253-257.
17. Gundberg CM, Markowitz ME, Mizruchi M, Rosen JF: **Osteocalcin in human serum: a circadian rhythm.** *J Clin Endocrinol Metab* 1985, **60**:736-739.
18. Halleen JM, Alatalo SL, Suominen H, Cheng S, Janckila AJ, Väänänen HK: **Tartrate-resistant acid phosphatase 5b: a novel serum marker of bone resorption.** *J Bone Miner Res* 2000, **15**:1337-1345.
19. Lacey DL, Timms E, Tan HL, Kelley MJ, Dunstan CR, Burgess T, *et al*: **Osteoprotegerin ligand is a cytokine that regulates osteoclast differentiation and activation.** *Cell* 1998, **93**:165-176.
20. Tanaka S, Nakamura K, Takahasi N, Suda T: **Role of RANKL in physiological and pathological bone resorption and therapeutics targeting the RANKL-RANK signaling system.** *Immunol Rev* 2005, **208**:30-49, Review.
21. Ealey KN, Kaludjerovic J, Archer MC, Ward WE: **Adiponectin is a negative regulator of bone mineral and bone strength in growing mice.** *Exp Biol Med (Maywood)* 2008, **233**:1546-1553.
22. Waki H, Yamauchi T, Kamon J, Ito Y, Uchida S, Kita S, *et al*: **Impaired multimerization of human adiponectin mutants associated with diabetes. Molecular structure and multimer formation of adiponectin.** *J Biol Chem* 2003, **278**:40352-40363.
23. Tsao TS, Tomas E, Murrey HE, Hug C, Lee DH, Ruderman NB, *et al*: **Role of disulfide bonds in Acrp30/adiponectin structure and signaling specificity. Different oligomers activate different signal transduction pathways.** *J Biol Chem* 2003, **278**:50810-50817.
24. Williams GA, Wang Y, Callon KE, Watson M, Lin JM, Lam JB, *et al*: **In vitro and in vivo effects of adiponectin on bone.** *Endocrinology* 2009, **150**:3603-3610.
25. Maeda N, Shimomura I, Kishida K, Nishizawa H, Matsuda M, Nagaretani H, *et al*: **Diet-induced insulin resistance in mice lacking adiponectin/ACRP30.** *Nat Med* 2002, **8**:731-737.
26. Yano W, Kubota N, Itoh S, Kubota T, Awazawa M, Moroi M, *et al*: **Molecular mechanism of moderate insulin resistance in adiponectin-knockout mice.** *Endocr J* 2008, **55**:515-522.
27. Nakayama H, Otabe S, Yuan X, Ueno T, Hirota N, Fukutani T, *et al*: **Effects of adiponectin transgenic expression in liver of nonalcoholic steatohepatitis model mice.** *Metabolism* 2009, **58**:901-908.
28. Almeida M, Han L, Martin-Millan M, Plotkin LI, Stewart SA, Roberson PK, *et al*: **Skeletal involution by age-associated oxidative stress and its acceleration by loss of sex steroids.** *J Biol Chem* 2007, **282**:27285-27297.
29. Kadowaki T, Tobe K, Honda-Yamamoto R, Tamemoto H, Kaburagi Y, Momomura K, *et al*: **Signal transduction mechanism of insulin and insulin-like growth factor-1.** *Endocr J* 1996, **43**:S33-41.
30. Sun XJ, Pons S, Wang LM, Zhang Y, Yenush L, Burks D, *et al*: **The IRS-2 gene on murine chromosome 8 encodes a unique signaling adapter for insulin and cytokine action.** *Mol Endocrinol* 1997, **11**:251-262.
31. Fiorelli G, Formigli L, Zecchi Orlandini S, Gori F, Falchetti A, Morelli A, *et al*: **Characterization and function of the receptor for IGF-I in human preosteoclastic cells.** *Bone* 1996, **18**:269-276.
32. Hou P, Sato T, Hofstetter W, Foged NT: **Identification and characterization of the insulin-like growth factor I receptor in mature rabbit osteoclasts.** *J Bone Miner Res* 1997, **12**:534-540.

Pre-publication history
The pre-publication history for this paper can be accessed here:
http://www.biomedcentral.com/1471-2474/12/18/prepub

doi:10.1186/1471-2474-12-18
Cite this article as: Mitsui *et al.*: Hyperadiponectinemia enhances bone formation in mice. *BMC Musculoskeletal Disorders* 2011 **12**:18.

J Shoulder Elbow Surg (2011) ■, 1-6

ELSEVIER

JOURNAL OF SHOULDER AND ELBOW SURGERY

www.elsevier.com/locate/ymse

Infraspinatus fatigue during resisted arm elevation with isometric contraction: an electromyographic study

Yoshihiro Kai, PT, MS[a], Masafumi Gotoh, MD, PhD[b,*], Kensei Nagata, MD, PhD[c], Naoto Shiba, MD, PhD[d]

[a]*Kurume University School of Medicine Graduate School, Asahi-machi, Kurume, Fukuoka, Japan*
[b]*Department of Orthopedic Surgery, Kurume University Medical Center, Kokubu-machi, Kurume, Fukuoka, Japan*
[c]*Department of Orthopedic Surgery, Kurume University, Asahi-machi, Kurume, Fukuoka, Japan*
[d]*Division of Rehabilitation, Kurume University, Asahi-machi, Kurume, Fukuoka, Japan*

Background: Various forms of resistance are used in rotator cuff training programs. However, the muscular activity of the infraspinatus during arm elevation has not been clarified in detail. We aimed to evaluate infraspinatus fatigue during resisted arm elevation in various positions.

Methods: The dominant (right) shoulders of 39 healthy subjects were examined. Average mean power frequency shifts of the infraspinatus and deltoid were evaluated electromyographically when the subjects performed isometric contractions equivalent to 30% of the maximal voluntary isometric contraction force for 60 s during 90° arm elevation in the sagittal and scapular planes, prone and side-lying external rotations, and repeated side-lying external rotation exercise. Further, the arm-elevation force was measured before and after the repeated external rotation exercise. Analysis of variance and paired t tests were used for statistical analyses; differences at $P < .05$ were considered significant.

Results: The infraspinatus was fatigued easily during resisted arm elevation in the sagittal plane compared with the scapular plane ($P < .01$). Comparisons of sagittal-plane elevation with side-lying and prone external rotations revealed no significant differences in the fatigue levels. The arm-elevation force after the repeated external rotations was significantly decreased in the sagittal plane compared with the scapular plane ($P < .01$).

Conclusion: In clinical settings, this data may be helpful in knowing how to helpful to protect the infraspinatus after surgical repair. Therefore, therapeutic exercise regimes with resisted arm elevation should avoid infraspinatus overfatigue in the sagittal plane in the early postoperative period.

Level of evidence: Basic Science Study, Kinesiology Study.

Keywords: Infraspinatus; muscular fatigue; arm elevation; electromyography; mean power frequency; repetitive external rotation; therapeutic exercise; biomechanics

The infraspinatus acts as an external rotator to stabilize the glenohumeral joint.[7,8,18,35] Several researchers have indicated that this muscle also contributes to arm elevation.[19,26,30] A recent anatomical study has demonstrated that the infraspinatus occupies about half of the highest impression on the greater tuberosity, which was believed to be the footprint of the

IRB approval: The Institutional Review Board of Kurume University approved the study protocol (#07114) and all subjects gave their written informed consent for participation in the study.

*Reprint requests: Masafumi Gotoh, MD, PhD, Department of Orthopedic Surgery, Kurume University Medical Center, 155-1 Kokubu-machi, Kurume, Fukuoka 839-0863, Japan.

E-mail address: gomasa@kurume.med-u.ac.jp (M. Gotoh).

1058-2746/$ - see front matter © 2011 Journal of Shoulder and Elbow Surgery Board of Trustees.
doi:10.1016/j.jse.2011.07.021

supraspinatus, thus supporting the concept that the infraspinatus contributes more to arm elevation than previously believed.[24]

The scapular plane has been identified as the most efficient plane for the arm-elevation maneuver.[15] According to Johnston,[15] scapular-plane elevation allows the arm to achieve the full benefit of scapular rotation. He also believed that the arm experiences the least fatigue in this position, because of the relaxed orientation of the deltoid and rotator cuff muscles and the untwisted configuration of the inferior joint capsule.[15,28] It is also the ideal position to obtain full postoperative passive range of motion without stressing the capsular or musculotendinous repair.[1] Consequently, isotonic rehabilitation exercise for the rotator cuff and deltoid muscles is commonly performed in the scapular plane.[31]

Surface electromyography (EMG) is a valid and reliable tool to measure muscle fatigue.[9,16,20,22,25] Although surface EMG has limitations related to electrode placement, skin impedance, and cross-talk, it has been used to evaluate the degree of fatigue of different muscles.[21,25] Hagberg[13] found a mean power frequency (MPF) decrease in a fatiguing contraction due to alterations in the muscle energy metabolism; this decrease in the conduction velocity of the muscle fibers causes a shift in the power spectra toward lower frequencies. Similarly, Gerdle et al[12] demonstrated that MPF shifts are consistent with mechanical muscular fatigue and associated with a considerable degree of local muscular fatigue; they also showed that the fatiguing phase correlates with an increasing degree of fatigue of type-II motor units.

Biomechanical/EMG studies have focused on the infraspinatus activity during arm elevation in the scapular or coronal plane,[1,17,23,26,30,31,34] but not on its activity during arm elevation in the sagittal plane. Considering that assessment of infraspinatus activity will enhance our understanding of the muscle function during arm movements, we aimed to evaluate infraspinatus fatigue during resisted isometric arm elevation in various positions by EMG. Our hypothesis was that during resisted arm elevation, the infraspinatus is fatigued easier in the sagittal plane than in the scapular plane.

Materials and methods

Subjects

We examined the dominant shoulders of 39 right-handed subjects. No subject had any history of shoulder pain or injuries before participating in this study. Their mean age was 21.2 years (range, 20–26), mean height was 170.7 cm (range, 159–178), and mean weight was 62.8 kg (range, 55–68).

Experimental procedures

Infraspinatus and deltoid activities were recorded by EMG. The electrode placement locations were selected according to published studies involving EMG data collection from the muscles of interest.[27] For the infraspinatus, electrodes were placed 2 fingerbreadths inferior to the center of the spina scapulae. For the anterior deltoid, electrodes were placed three fingerbreadths inferior to the anterior border of the acromion process. For the middle deltoid, electrodes were placed midway between the deltoid tuberosity and the acromion process. For the posterior deltoid, electrodes were placed 2 fingerbreadths inferior to the posterior margin of the acromion process. A ground electrode was placed on the acromion process.

MyoSystem 1200 (Noraxon U.S.A., Inc, Scottsdale, AZ, USA) was used to collect raw surface EMG data. This unit provides signal amplification of 1000×, 20–500 Hz band-pass filtering, a common-mode rejection ratio greater than 100 dB, and input impedance greater than 10 MΩ. Output from the unit was linked to a 16-bit analog-to-digital converter in a personal computer, and the raw data were monitored and collected in MyoResearch 2.11 (Noraxon U.S.A., Inc) at 1024 Hz. The skin was prepared by scrubbing the area with alcohol pads, and the electrodes were applied parallel to the muscle fibers. Self-adhesive bipolar surface electrodes (Medicotest Blue Sensor, Chicago, IL, USA) were then attached. Correct electrode placement was confirmed by observing all EMG signals on an oscilloscope during resisted contractions of each muscle.

Force loading

Each subject was seated upright on a chair. Then, force loading was applied with the shoulder at 90° elevation in the sagittal or scapular plane and the elbow extended 0° with the forearm midway between the thumb-up and thumb-down positions (Fig. 1, *A-D*). Force loading was also applied during side-lying external rotation (ER) supported by a towel roll with the arm abducted at 10–20° and the elbow flexed at 90°,[6] and during prone ER with the arm abducted at 90° and externally rotated at 90°.[6] Shoulder muscular fatigue was measured when the subjects performed isometric contractions equivalent to 30% of the maximal voluntary isometric contraction (MVIC) force for 60 sec in the described positions.

The MVIC force was measured twice by a PowerTrack II Commander handheld dynamometer (JTech Medical Industries, Salt Lake City, UT, USA) before this experiment. The sensor pad of the handheld dynamometer was placed on the distal forearm and fixed with a strap. A posture hold bar and cephalic strap were used to minimize motion during the experiment. The mean value of the two trials at 100% MVIC force was obtained and the 30% MVIC force was then calculated.

Repeated ER exercise

Repeated ER exercise was performed according to the method of Wakabayashi et al.[33] In brief, side-lying ERs were performed repeatedly with a dumbbell of 3 kg, until at least 30% reduction in the maximum ER force was achieved. Before and after this exercise, the arm-elevation force in the sagittal and scapular planes was measured by the dynamometer in the same position as already described. Then, changes in the arm-elevation force before and after the exercise were calculated.

Data reduction

Muscular fatigue was defined as a decrease in MPF output over time. The MPF was derived from the raw EMG data by using

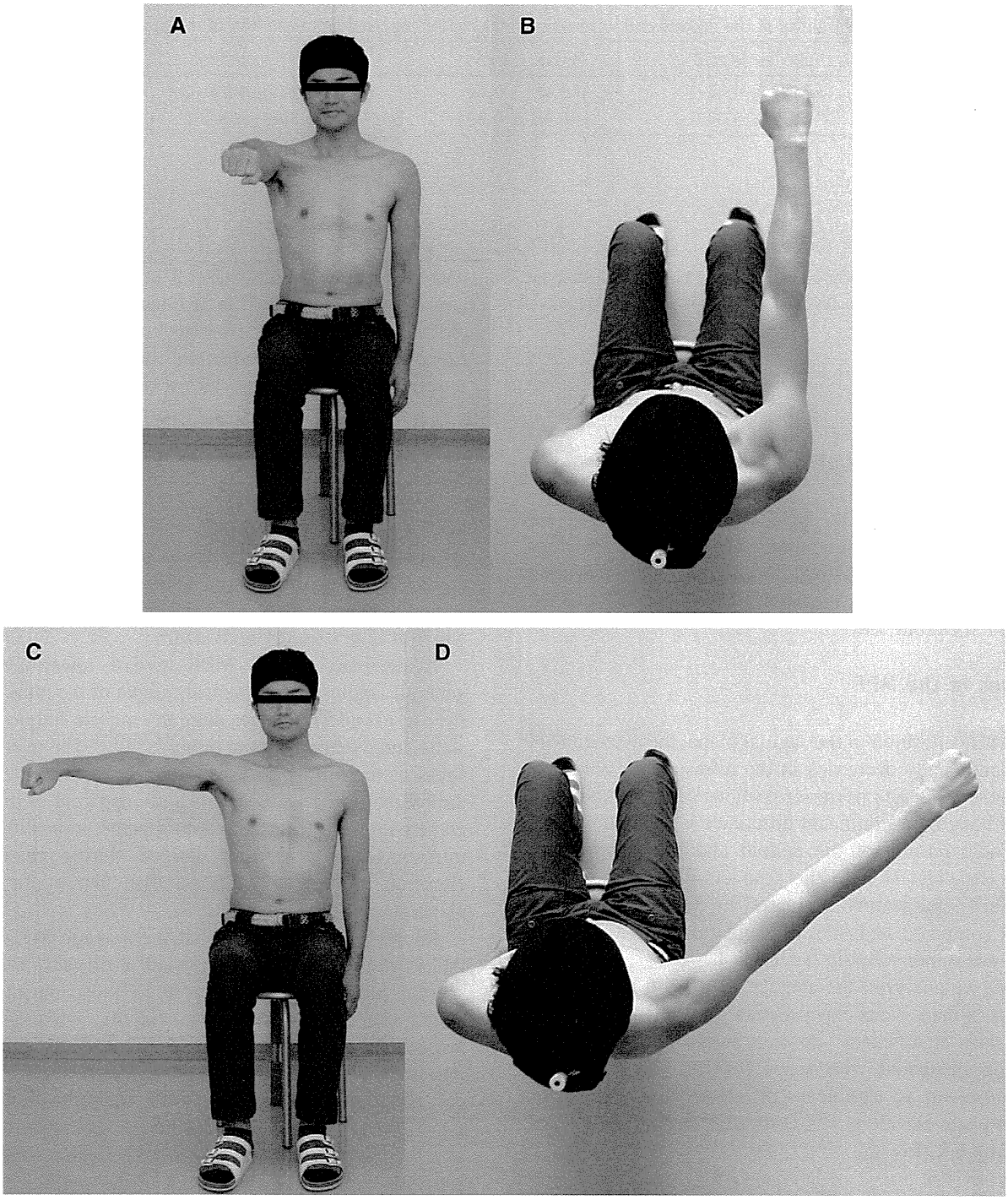

Figure 1 Experimental view. The force loading was applied with the shoulder at 90° elevation in the sagittal (**A, B**) and scapular plane (**C, D**).

the Fast Fourier Transformation (FFT) algorithm. The EMG data were separated into 1-sec intervals and entered into the algorithm to establish the power density spectrum, which was then used to determine the MPF for each 1-sec interval over a 60-sec period. Least-squares regression analysis was used to determine the linear decline in the MPF slope for each muscle over time and identify differences in the MPF output per muscle.

Statistical analysis

StatView 5.0 (SAS Institute, Inc, Cary, NC, USA) was used to compute a mixed linear model for repeated-measures analysis of variance (ANOVA) of each slope of muscular fatigue and determine differences in the fatigue level. Post hoc analysis was then performed through Scheffe's correction. Paired *t* tests were used to

Table I The average MPF shifts of the deltoid and infraspinatus during 90° resisted arm elevation in the sagittal and scapular planes

	Anterior deltoid	Middle deltoid	Posterior deltoid	Infraspinatus
Sagittal plane	−0.31 ± 0.04	−0.42 ± 0.04	−0.26 ± 0.03	−0.51 ± 0.05**
Scapular plane	−0.36 ± 0.03*	−0.38 ± 0.03**	−0.30 ± 0.04	−0.20 ± 0.04

* $P < .05$.
** $P < .01$.

compare changes in the arm-elevation force before and after the repeated ER exercise. The level of significance for all statistical testing was $P < .05$.

Results

Intrarater reliability of the MVIC force

Intrarater reliability of the MVIC force measurement was analyzed by using intraclass correlation coefficients (ICC).[1,2] The ICC was 0.94 for sagittal-plane elevation, 0.98 for scapular-plane elevation, 0.96 for side-lying ER, and 0.97 for prone ER.

Changes in the MPF

During arm elevation in the sagittal plane, the average MPF shift significantly decreased in the infraspinatus compared with the anterior and posterior portions of the deltoid ($P < .05$); although, no significant difference was noted between the middle portion of the deltoid and the infraspinatus. During arm elevation in the scapular plane, the average MPF shift significantly decreased in each portion of the deltoid compared with the infraspinatus ($P < .01$). These results are summarized in the Table I.

Next, we analyzed the average MPF shift of the infraspinatus in the various experimental positions. The average MPF shift significantly decreased during sagittal-plane elevation compared with scapular-plane elevation ($P < .01$). However, no significant difference was noted when sagittal-plane elevation was compared with prone ER and side-lying ER (Fig. 2).

Changes in the arm-elevation force with repeated ER exercise

To begin with, the average MPF shift of the deltoid and infraspinatus was evaluated before and after the repeated ER exercise. The average MPF shift significantly decreased in the infraspinatus ($P < .01$), but did not significantly differ in any portion of the deltoid (Fig. 3).

Next, we analyzed the arm-elevation force in the sagittal and scapular planes before and after the repeated ER exercise. The force in the sagittal plane significantly decreased after the exercise (143.3 ± 19.6 N) compared with before the exercise (201.5 ± 27.9 N). Although the arm-elevation force in the scapular plane also decreased (130.4 ± 18.6 N post-exercise vs. 163.0 ± 19.1 N pre-exercise), its rate of reduction was less than that in the sagittal plane (−19.8 ± 9.1% vs −28.5 ± 7.8%; Fig. 4).

Discussion

MPF analysis in the present study elicited that the infraspinatus is fatigued easily during resisted arm elevation in the sagittal plane compared with the scapular plane, and shows a similar level of fatigue during resisted ERs in which it is maximally activated.

A decrease in the MPF toward lower frequencies generally indicates mechanical fatigue of the muscle.[11,12] A shift to lower frequencies suggests muscle fatigue for both static and dynamic contractions.[11,13,21,25] The average MPF shifts of the infraspinatus during resisted arm elevation in the present study were significantly apparent in the sagittal plane compared with the scapular plane, indicating that the infraspinatus has greater fatigue during resisted arm elevation in the sagittal plane than that in the scapular plane.

Interestingly, we found that the average MPF shifts of the infraspinatus during resisted arm elevation in the sagittal plane were comparable to those during ERs in which the infraspinatus is maximally activated.[3,29] The infraspinatus is not only an external rotator but also an important stabilizer of the glenohumeral joint.[5,6,18,35] As part of the transverse force couple, the infraspinatus fulfils a primary stabilizing role around the shoulder rather than a principle torque-producing role.[4] Taken together, we conclude that the arm elevation in the sagittal plane may lead to considerable muscle fatigue of the infraspinatus as caused during external rotation.

The mean fiber proportions determine the extent of muscular fatigue. Predominantly tonic muscles have a higher percentage of type-I fibers and predominantly phasic muscles have a higher percentage of type-II fibers.[14] Considering that type-II fibers fatigue more easily than type-I fibers, muscles with a larger proportion of type-II fibers would have a greater decrease in MPF.[16] Furthermore, another study has shown that MPF decreases in EMG analysis reflect fatigue of type-II muscle fibers.[12] An immunohistochemical study demonstrated that the

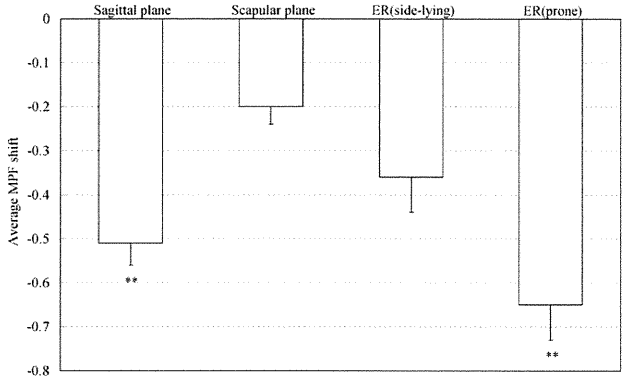

Figure 2 Comparison of the average MPF shifts of the infraspinatus in the various experimental positions. *ER*, external rotation; $**P < .01$.

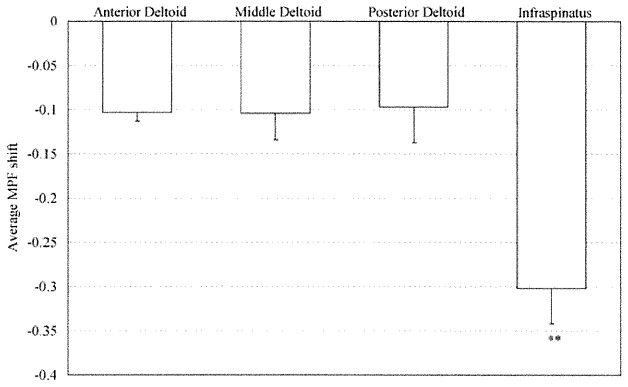

Figure 3 Comparison of the average MPF shifts of the deltoid and infraspinatus after repeated side-lying external rotations. $**P < .01$.

infraspinatus and deltoid have a similar proportion of type-II fibers (~60%).[14] Therefore, comparison of MPF shifts between these muscles is thought to be a valid analytical method.

Previous studies have documented that ER positions result in a high level of deltoid activation,[3,10,29] and side-lying ER exercise reportedly activates the middle and posterior deltoid portions the least compared with other ER exercises.[3] In the present study, we noted a significant decrease in the average MPF shift of the infraspinatus, but not in any portion of the deltoid, after repeated side-lying ER exercise. Furthermore, this fatigue-inducing exercise led to a significant decrease in the resisted arm-elevation force in the sagittal plane compared with the scapular plane. These results indicate that the fatigue-inducing exercise preferentially caused infraspinatus fatigue but not deltoid fatigue, and therefore support the idea that the infraspinatus is fatigued to a greater extent during sagittal-plane elevation than during scapular-plane elevation.

The present study has several limitations. First, the measurements were limited to 1 position, with the arm elevated at 90° in the sagittal and scapular planes. The muscle intensity peaks at 88° and 105° arm elevation,[34] and

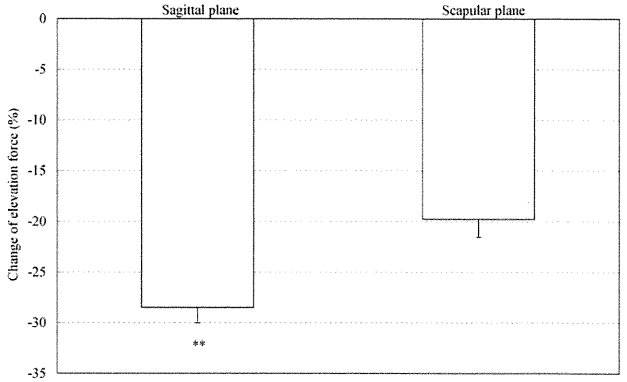

Figure 4 Changes in the arm-elevation force of the infraspinatus in the sagittal and scapular planes after repeated side-lying external rotations. The changes were calculated as the relative ratio (%) of the pre-exercise force to the post-exercise force. $**P < .01$.

the gravity torque and joint-compressive loads are the greatest at 90° arm elevation.[2] Therefore, we considered the position of 90° arm elevation in the sagittal and scapular planes as the most appropriate to evaluate muscular fatigue. Second, we did not examine the supraspinatus as a prime mover during arm elevation; instead, the deltoid, another prime mover during arm elevation, was examined. Because the use of surface electrodes to estimate indwelling rotator cuff activity is cautioned against,[32] analysis with fine-wire electrodes may have been needed in the present study. Third, we did not support the scapula while performing the experiments, which might have affected the present data. Finally, the supraspinatus and the teres minor were not examined in the repeated ER exercise, despite their association with the external rotation.[5] Resolving these issues could lead to better understanding of muscular fatigue during arm elevation.

Conclusion

During resisted arm elevation with isometric contraction, the infraspinatus is fatigued more easily in the sagittal plane than in the scapular plane. In clinical settings, this data may be helpful in knowing how to helpful to protect the infraspinatus after surgical repair. Therefore, therapeutic exercise regimes with resisted arm elevation should avoid infraspinatus overfatigue in the sagittal plane in the early postoperative period.

Disclaimer

None of the authors, their immediate families, and any research foundation with which they are affiliated received any financial payments or other benefits from any commercial entity related to the subject of this article.

References

1. Alpert SW, Pink MM, Jobe FW, McMahon PJ, Mathiyakom W. Electromyographic analysis of deltoid and rotator cuff function under varying loads and speeds. J Shoulder Elbow Surg 2000;9:47-58.
2. Antony NT, Keir PJ. Effects of posture, movement and hand load on shoulder muscle activity. J Electromyogr Kinesiol 2010;20:191-8. doi: 10.1016/j.jelekin.2009.04.010
3. Ballantyne BT, O'Hare SJ, Paschall JL, Pavia-Smith MM, Pitz AM, Gillon JF, et al. Electromyographic activity of selected shoulder muscles in commonly used therapeutic exercises. Phys Ther 1993;73:668-82.
4. Bitter NL, Clisby EF, Jones MA, Magarey ME, Jaberzadeh S, Sandow MJ. Relative contributions of infraspinatus and deltoid during external rotation in healthy shoulders. J Shoulder Elbow Surg 2007;16: 563-8. doi:10.1016/j.jse.2006.11.007
5. Blonna D, Cecchetti S, Tellini A, Bonasia DE, Rossi R, Southgate R, et al. Contribution of the supraspinatus to the external rotator lag sign: kinematic and electromyographic pattern in an in vivo model. J Shoulder Elbow Surg 2010;19:392-8. doi:10.1016/j.jse.2009.10.007
6. Brookham RL, McLean L, Dickerson CR. Construct validity of muscle force tests of the rotator cuff muscles: an electromyographic investigation. Phys Ther 2010;90:572-80. doi:10.2522/ptj.20090024
7. Burkhart SS. Arthroscopic treatment of massive rotator cuff tears. Clinical results and biomechanical rationale. Clin Orthop Relat Res 1991;267:45-56.
8. Cain PR, Mutschler TA, Fu FH, Lee SK. Anterior stability of the glenohumeral joint. A dynamic model. Am J Sports Med 1987;15:144-8.
9. Christova P, Kossev A, Kristev I, Chichov V. Surface EMG recorded by branched electrodes during sustained muscle activity. J Electromyogr Kinesiol 1999;9:263-76.
10. Clisby EF, Bitter NL, Sandow MJ, Jones MA, Magarey ME, Jaberzadeh S. Relative contributions of the infraspinatus and deltoid during external rotation in patients with symptomatic subacromial impingement. J Shoulder Elbow Surg 2008;17:87S-92S. doi:10.1016/j.jse.2007.05.019
11. Gerdle B, Edström M, Rahm M. Fatigue in the shoulder muscles during static work at two different torque levels. Clin Physiol 1993;13: 469-82.
12. Gerdle B, Elert J, Henriksson-Larsén K. Muscular fatigue during repeated isokinetic shoulder forward flexions in young females. Eur J Appl Physiol Occup Physiol 1989;58:666-73.
13. Hagberg M. Muscular endurance and surface electromyogram in isometric and dynamic exercise. J Appl Physiol 1981;51:1-7.
14. Johnson M, Polgar J, Weightman D, Appleton D. Data on the distribution of fiber types in thirty-six human muscles: an autopsy study. J Neurol Sci 1973;18:111-29.
15. Johnston TB. The movements of the shoulder joint: a plea for the use of the "plane of the scapula" as the plane of reference for movements occurring at the humero-scapular joint. Br J Surg 1937;25:252-60.
16. Komi PV, Tesch P. EMG frequency spectrum, muscle structure, and fatigue during dynamic contractions in man. Eur J Appl Physiol Occup Physiol 1979;42:41-50.
17. Kronberg M, Németh G, Broström LA. Muscle activity and coordination in the normal shoulder. An electromyographic study. Clin Orthop Relat Res 1990;257:76-85.
18. Lee SB, Kim KJ, O'Driscoll SW, Morrey BF, An KN. Dynamic glenohumeral stability provided by the rotator cuff muscles in the mid-range and end-range of motion. A study in cadavera. J Bone Joint Surg Am 2000;82:849-57.
19. Liu J, Hughes RE, Smutz WP, Niebur G, Nan-An K. Roles of deltoid and rotator cuff muscles in shoulder elevation. Clin Biomech (Bristol, Avon) 1997;12:32-8.
20. Ludewig PM, Cook TM, Nawoczenski DA. Three-dimensional scapular orientation and muscle activity at selected positions of humeral elevation. J Orthop Sports Phys Ther 1996;24:57-65.
21. McQuade KJ, Dawson J, Smidt GL. Scapulothoracic muscle fatigue associated with alterations in scapulohumeral rhythm kinematics during maximum resistive shoulder elevation. J Orthop Sports Phys Ther 1998;28:74-80.
22. Merletti R, Lo Conte LR. Surface EMG signal processing during isometric contractions. J Electromyogr Kinesiol 1997;7:241-50.
23. Minning S, Eliot CA, Uhl TL, Malone TR. EMG analysis of shoulder muscle fatigue during resisted isometric shoulder elevation. J Electromyogr Kinesiol 2007;17:153-9. doi:10.1016/j.jelekin.2006.01.008
24. Mochizuki T, Sugaya H, Uomizu M, Maeda K, Matsuki K, Sekiya I, et al. Humeral insertion of the supraspinatus and infraspinatus. New anatomical findings regarding the footprint of the rotator cuff. J Bone Joint Surg Am 2008;90:962-9. doi:10.2106/JBJS.G.00427
25. Moritani T, Muro M, Nagata A. Intramuscular and surface electromyogram changes during muscle fatigue. J Appl Physiol 1986;60: 1179-85.
26. Otis JC, Jiang CC, Wickiewicz TL, Peterson MG, Warren RF, Santner TJ. Changes in the moment arms of the rotator cuff and deltoid muscles with abduction and rotation. J Bone Joint Surg Am 1994;76:667-76.
27. Perotto A. Anatomical Guide for the Electromyographer: The Limbs and Trunk. 3rd ed. Springfield, IL: Charles C Thomas; 1994 (ISBN: 978–0398059002).
28. Poppen NK, Walker PS. Normal and abnormal motion of the shoulder. J Bone Joint Surg Am 1976;58:195-201.
29. Reinold MM, Wilk KE, Fleisig GS, Zheng N, Barrentine SW, Chmielewski T, et al. Electromyographic analysis of the rotator cuff and deltoid musculature during common shoulder external rotation exercises. J Orthop Sports Phys Ther 2004;34:385-94.
30. Sharkey NA, Marder RA, Hanson PB. The entire rotator cuff contributes to elevation of the arm. J Orthop Res 1994;12:699-708.
31. Vailas JC, Morris M, Pink M, Perry J, Jobe FW. Muscle activity during isotonic, variable resistance, and isokinetic exercise. Clin J Sport Med 1992;2:186-91.
32. Waite DL, Brookham RL, Dickerson CR. On the suitability of using surface electrode placements to estimate muscle activity of the rotator cuff as recorded by intramuscular electrodes. J Electromyogr Kinesiol 2010;20:903-11. doi:10.1016/j.jelekin.2009.10.003
33. Wakabayashi I, Itoi E, Shimizu T. The effect of external rotator muscle fatigue on humeral head centralization during arm elevation [in Japanese]. Shoulder Joint 2001;25:263-6.
34. Wickham J, Pizzari T, Stansfeld K, Burnside A, Watson L. Quantifying 'normal' shoulder muscle activity during abduction. J Electromyogr Kinesiol 2010;20:212-22. doi:10.1016/j.jelekin.2009.06.004
35. Wuelker N, Korell M, Thren K. Dynamic glenohumeral joint stability. J Shoulder Elbow Surg 1998;7:43-52.

Published October 17, 2011

Correction

The Journal of Experimental Medicine

Osteoclasts are dispensable for hematopoietic stem cell maintenance and mobilization

Kana Miyamoto, Shigeyuki Yoshida, Miyuri Kawasumi, Kazuaki Hashimoto, Tokuhiro Kimura, Yuiko Sato, Tami Kobayashi, Yoshiteru Miyauchi, Hiroko Hoshi, Ryotaro Iwasaki, Hiroya Miyamoto, Wu Hao, Hideo Morioka, Kazuhiro Chiba, Takashi Kobayashi, Hisataka Yasuda, Josef M. Penninger, Yoshiaki Toyama, Toshio Suda, and Takeshi Miyamoto

Vol. 208, No. 11, October 24, 2011. Pages 2175–2181.

The authors regret that the dosage of RANKL and control antibodies used in the HSC mobilization experiments shown in Figure 6 were incorrectly reported in micrograms. The correct dosages were 5 mg/kg anti-RANKL and 2.5 mg/kg control antibody. The html and pdf versions of the article have been corrected.

Published October 17, 2011

JEM

Brief Definitive Report

Osteoclasts are dispensable for hematopoietic stem cell maintenance and mobilization

Kana Miyamoto,[1,2] Shigeyuki Yoshida,[3,4] Miyuri Kawasumi,[2] Kazuaki Hashimoto,[1,5] Tokuhiro Kimura,[6] Yuiko Sato,[1,7] Tami Kobayashi,[1,2] Yoshiteru Miyauchi,[1,4] Hiroko Hoshi,[1,4] Ryotaro Iwasaki,[3] Hiroya Miyamoto,[1,4] Wu Hao,[1] Hideo Morioka,[1] Kazuhiro Chiba,[1] Takashi Kobayashi,[2] Hisataka Yasuda,[9] Josef M. Penninger,[10] Yoshiaki Toyama,[1] Toshio Suda,[8] and Takeshi Miyamoto[1,2,4,5,11]

[1]Department of Orthopedic Surgery, [2]Keio Kanrinmaru Project, [3]Department of Dentistry and Oral Surgery, [4]Center for Human Metabolomic Systems Biology, [5]Department of Integrated Bone Metabolism and Immunology, [6]Department of Pathology, [7]Department of Musculoskeletal Reconstruction and Regeneration Surgery, and [8]Department of Cell Differentiation, Keio University School of Medicine, Shinjuku-ku, Tokyo 160-8582, Japan
[9]Bioindustry Division, Oriental Yeast Co., Itabashi-ku, Tokyo 174-8505, Japan
[10]Institute of Molecular Biotechnology of the Austrian Academy of Sciences, 1030 Vienna, Austria
[11]Precursory Research for Embryonic Science and Technology, Japan Science and Technology Agency, Kawaguchi, Saitama 332-0012, Japan

Hematopoietic stem cells (HSCs) are maintained in a specific bone marrow (BM) niche in cavities formed by osteoclasts. Osteoclast-deficient mice are osteopetrotic and exhibit closed BM cavities. Osteoclast activity is inversely correlated with hematopoietic activity; however, how osteoclasts and the BM cavity potentially regulate hematopoiesis is not well understood. To investigate this question, we evaluated hematopoietic activity in three osteopetrotic mouse models: *op/op*, c-Fos-deficient, and RANKL (receptor activator of nuclear factor kappa B ligand)-deficient mice. We show that, although osteoclasts and, by consequence, BM cavities are absent in these animals, hematopoietic stem and progenitor cell (HSPC) mobilization after granulocyte colony-stimulating factor injection was comparable or even higher in all three lines compared with wild-type mice. In contrast, osteoprotegerin-deficient mice, which have increased numbers of osteoclasts, showed reduced HSPC mobilization. BM-deficient patients and mice reportedly maintain hematopoiesis in extramedullary spaces, such as spleen; however, splenectomized *op/op* mice did not show reduced HSPC mobilization. Interestingly, we detected an HSC population in osteopetrotic bone of *op/op* mice, and pharmacological ablation of osteoclasts in wild-type mice did not inhibit, and even increased, HSPC mobilization. These results suggest that osteoclasts are dispensable for HSC mobilization and may function as negative regulators in the hematopoietic system.

CORRESPONDENCE
T. Miyamoto:
miyamoto@z5.keio.jp

Abbreviations used: 5-FU, 5-fluorouracil; BMD, bone mineral density; HSC, hematopoietic stem cell; HSPC, hematopoietic stem and progenitor cell; LSK, lineage negative, c-Kit positive, and Sca1 positive; OPG, osteoprotegerin; RANKL, receptor activator of nuclear factor kappa B ligand.

Hematopoietic stem cells (HSCs) have the ability to self-renew as well as to produce multiple lineages of daughter cells throughout an animal's life (Adams and Scadden, 2006; Kiel and Morrison, 2008). Hematopoietic stem and progenitor cells (HSPCs) are thought to reside in specific niches, which are specialized microenvironments within the BM cavity (Calvi et al., 2003; Zhang et al., 2003; Arai et al., 2004; Kiel et al., 2005; Stier et al., 2005; Adams and Scadden, 2006; Sugiyama et al., 2006; Kiel and Morrison, 2008; Lymperi et al., 2010). Niches consist of various cell types such as osteoblastic cells, vascular endothelial cells or reticular cells, and associated factors such as angiopoietin1, N-cadherin, osteopontin, and Cxcl12 (Calvi et al., 2003; Zhang et al., 2003; Arai et al., 2004; Kiel et al., 2005; Stier et al., 2005; Adams and Scadden, 2006; Sugiyama et al., 2006; Kiel and Morrison, 2008; Lymperi et al., 2010). A functional BM is reportedly required for HSPC mobilization to the periphery from BM cavities (Katayama et al., 2006). Thus, these cavities are considered crucial for HSPC

The Rockefeller University Press $30.00
J. Exp. Med. Vol. 208 No. 11 2175-2181
www.jem.org/cgi/doi/10.1084/jem.20101890

Published October 17, 2011

maintenance and mobilization; however, the impact of loss of BM cavities on the hematopoietic system remains unclear.

BM cavities are formed by osteoclasts, which are bone resorbing multinuclear cells, and loss of osteoclasts results in loss of BM cavities (Yoshida et al., 1990; Grigoriadis et al., 1994; Kong et al., 1999). Various factors, such as M-CSF, c-Fos, and receptor activator of nuclear factor kappa B ligand (RANKL), are reportedly essential for osteoclastogenesis; mutational inactivation or genetic ablation of these molecules results in a lack of osteoclast differentiation and consequent defects in BM cavity formation, a condition termed osteopetrosis in which BM cavities are filled with bone (Yoshida et al., 1990; Grigoriadis et al., 1994; Kong et al., 1999). Osteoprotegerin (OPG) is a decoy receptor of RANKL that inhibits osteoclastogenesis (Bucay et al., 1998; Mizuno et al., 1998). Although bone phenotypes of *op/op*, c-Fos–deficient, RANKL-deficient, and OPG-deficient mice have been described, hematopoietic phenotypes in these mice have not yet been fully characterized. Clinically, osteoclastic activity increases after serial G-CSF injection administered before peripheral HSC implantation (Takamatsu et al., 1998; Watanabe et al., 2003), and such activity is reportedly required to drive HSPCs from the marrow to the periphery (Kollet et al., 2006). Therefore osteoclast-deficient mice, which lack a BM niche, are predicted to be defective in hematopoiesis as a result of impaired osteoclast activity required to mobilize HSPCs to the periphery. Indeed, osteopetrotic patients, as well as animal models, reportedly show extramedullary hematopoiesis in the spleen (Freedman and Saunders, 1981; Lowell et al., 1996).

Osteoclastogenesis is accelerated with age, resulting in decreased bone mass (Manolagas and Jilka, 1995; Teitelbaum, 2007). Hematopoietic activity also decreases with age (Geiger and Rudolph, 2009; Waterstrat and Van Zant, 2009), suggesting that osteoclast activity is inversely correlated with hematopoietic activity; however, precise roles of osteoclasts in regulating hematopoiesis are largely unknown.

In this paper, we show that HSPCs are maintained even in osteopetrotic animals and that they are mobilized to the periphery after G-CSF stimulation, indicating that osteoclasts and BM cavities are both dispensable for HSPC maintenance and egress to the periphery. Pharmacological inhibition of osteoclastic activity did not inhibit but rather stimulated HSPC mobilization. Splenectomy of *op/op* mice increased HSPC mobilization, suggesting that spleen is not the primary tissue that maintains HSCs in osteopetrotic animals. HSCs were also detected in the osteopetrotic bone. OPG-deficient mice, which show increased osteoclastic activity, exhibited reduced HSPC mobilization. Thus, accelerated osteoclastic activity decreases both bone mass and hematopoietic activity, and both can be manipulated pharmacologically in vivo.

RESULTS AND DISCUSSION

HSPCs are maintained and mobilized in *op/op* mice

To determine whether loss of the BM niche and osteoclasts influences hematopoiesis, we analyzed osteopetrotic *op/op* mice, which carry a loss-of-function mutation in M-CSF, a cytokine essential for osteoclast differentiation (Yoshida et al., 1990). These mice lack a BM cavity and exhibit impaired osteoclastogenesis (Fig. 1 A). Previously, the cell cycle–specific cytotoxic agent 5-fluorouracil (5-FU), which is used in chemotherapy, has been used to evaluate HSC function because HSCs are resistant to 5-FU–induced cell death as a result of their quiescence (Cheng et al., 2000; Miyamoto et al., 2007). *op/op* and wild-type mice were serially treated with 5-FU, and we found that *op/op* mice were lethally susceptible to 5-FU treatment compared with control *op/+* mice (Fig. 1 B), suggesting that osteoclasts and BM cavities are required to maintain HSCs.

To confirm roles of osteoclasts and BM cavities in the hematopoietic system, *op/op* mice were serially treated with G-CSF and HSPCs mobilization was analyzed (Fig. 1, C–E). Because a functional BM niche or osteoclasts are reportedly required to mobilize HSPCs to the periphery from the BM (Heissig et al., 2002; Katayama et al., 2006; Kollet et al., 2006), we predicted that *op/op* mice would show inhibited HSPC mobilization after G-CSF injection. However, we found that mobilization of the HSC-enriched fraction (lineage negative, c-Kit positive, and Sca1 positive [LSK]) to peripheral blood, as analyzed by flow cytometry, was induced to levels even higher in *op/op* mice than in control littermate mice (*op/+*; Fig. 1, C and D). HSPCs mobilized in *op/op* mice were functional: colony-forming assays showed that greater numbers of colonies formed from the peripheral blood of G-CSF–treated *op/op* mice than from that of wild-type mice (Fig. 1 E). This observation suggests that *op/op* mice accumulate a greater number of HSCs than do wild-type mice, and that neither BM cavities nor osteoclasts are required for HSC maintenance and mobilization and may even be inhibitory to the process.

HSPC mobilization is induced in c-Fos– and RANKL-deficient mice

To confirm these findings, c-Fos–deficient mice, which are also osteoclast deficient and lack BM cavities, were analyzed (Fig. S1 A). We observed that c-Fos–deficient mice were less susceptible to serial 5-FU treatment than were *op/op* mice (Fig. S1 B), suggesting that M-CSF, rather than BM cavities and osteoclasts, is required to resist 5-FU treatment. Indeed, injection of M-CSF into *op/op* mice rescued mice from a lethal response to 5-FU (Fig. S1 C). M-CSF regulates osteoclast formation as well as macrophage differentiation and innate immunity (Miyamoto et al., 2001; Chitu and Stanley, 2006). In wild-type mice, M-CSF concentration in sera was significantly up-regulated after 5-FU treatment, suggesting a protective role for M-CSF against myelosuppression induced by chemotherapy (Fig. S1 D). In fact, both Gram-positive and -negative bacteria were detected in multiple organs of 5-FU–treated *op/op* mice (Fig. S1 E and not depicted). These results indicate that by inducing macrophages, M-CSF likely plays a critical role in resistance to hematopoietic suppression after 5-FU treatment. They also suggest that serum M-CSF concentrations should be carefully monitored during myelosuppressive chemotherapies to prevent opportunistic infections.

Published October 17, 2011

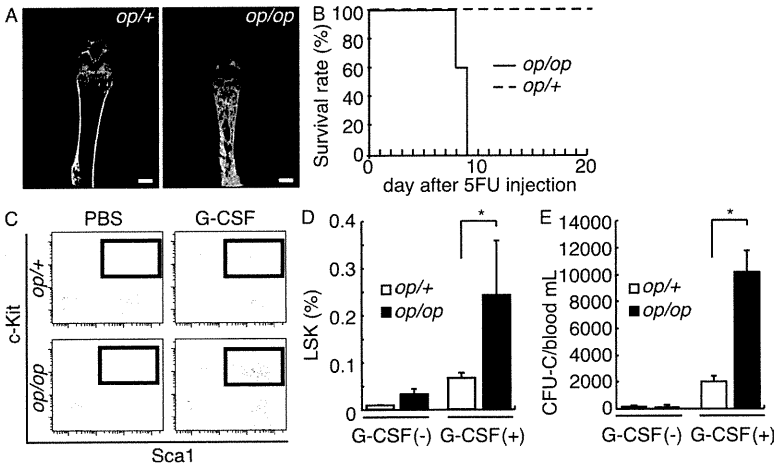

Figure 1. *op/op* mice are osteopetrotic and exhibit increased numbers of HSPCs. (A) Microradiographical analysis of femoral bones of 8-wk-old *op/op* and control (*op/+*) bone. Representative micro-CT data in three independent *op/op* or *op/+* mouse bones are shown. Bars, 1 mm. (B) 150 mg/kg 5-FU was injected into the peritoneal cavity of 8-wk-old *op/op* ($n = 5$) and littermate control (*op/+*; $n = 5$) mice on days 0 and 7, and the survival rate after 5-FU injection was analyzed. (C–E) 250 µg/kg/d G-CSF or PBS was injected subcutaneously into 8–12-wk-old *op/op* and control (*op/+*) mice daily for 5 d ($n = 3$ for each group). Peripheral blood was collected, and the frequency of the HSC fraction (LSK; C and D) and CFU-C (E) were analyzed. (C) Representative flow cytometric pattern of peripheral blood. Cells were gated on lineage (CD3, B220, TER119, Mac1, and Gr1)-negative cells. Data represent the mean LSK frequency (%) ± SD in peripheral blood (*, $P < 0.051$; D) and CFU-C ± SD in 1 ml peripheral blood (*, $P < 0.01$, $n = 9$ for each group; E). Representative data of three independent experiments are shown (B–E).

RANKL-deficient mice are also osteoclast deficient and lack BM cavities (Fig. S1 F). Interestingly, increased HSPC mobilization after serial G-CSF treatment was observed in both c-Fos–deficient and RANKL-deficient mice (Fig. 2), as it was in *op/op* mice, supporting the idea that osteoclasts and BM cavities are not required to maintain HSCs. Young female PTPε-knockout mice reportedly show a mild loss of osteoclast function but exhibit a BM cavity and impaired HSPC mobilization by G-CSF (Kollet et al., 2006). The three osteoclast- and BM cavity–deficient animal models evaluated in this study did not show defective HSPC mobilization after G-CSF treatment, suggesting that the function of osteoclasts in driving HSCs to the periphery is biphasic or BM cavity dependent. In wild-type mice, the number of osteoclasts reportedly does not increase during G-CSF treatment, but only after cessation of treatment (Takamatsu et al., 1998; Christopher and Link, 2008; Winkler et al., 2010), also suggesting that osteoclast loss likely does not affect HSPC mobilization in response to G-CSF treatment. All three osteopetrotic animal models show increased mobilization of HSPCs to the periphery without G-CSF administration (Figs. 1 and 2), suggesting that steady-state levels of circulating HSPCs are increased in these animals.

Impaired HSPC mobilization in OPG-deficient mice

To further explore the role of BM cavities and osteoclasts in HSC maintenance, HSPC mobilization in OPG-deficient mice was analyzed by serial G-CSF injection (Fig. 3). OPG is a decoy receptor for RANKL and therefore acts as a RANKL inhibitor (Bucay et al., 1998; Mizuno et al., 1998). OPG-deficient mice show severe osteoporosis as a result of accelerated osteoclastogenesis (Fig. 3, A and B). As expected, in contrast to osteoclast-deficient osteopetrotic mice, reduced HSPC mobilization was seen in OPG-deficient mice, as indicated by flow cytometry and colony-forming assays, compared with wild-type mice (Fig. 3, C–E). Furthermore, long-term competitive repopulation assays using mobilized cells from CD45.2$^+$ *op/op*, c-Fos–deficient, or RANKL-deficient mice versus CD45.1$^+$ BM competitors showed higher chimerism relative to that induced using mobilized cells from control mice (Fig. 3 F). In contrast, mobilized cells from OPG-deficient mice induced lower chimerism than those from wild-type mice (Fig. 3 F). CD45.2 reconstitution was multilineage; CD45.2 reconstitution from mobilized donor

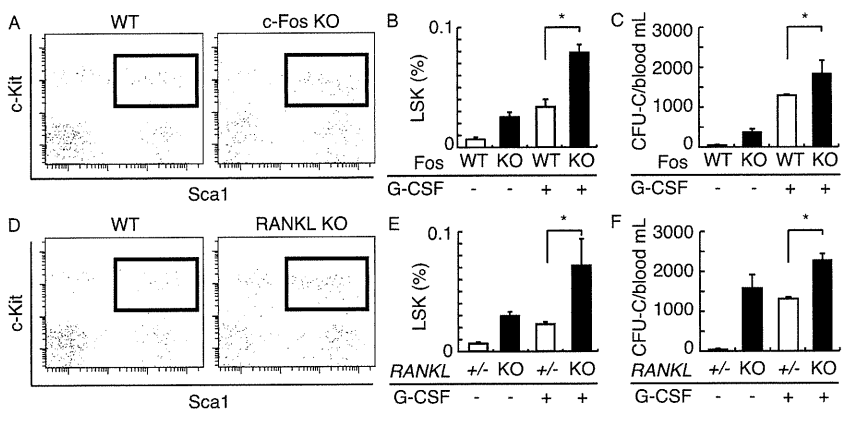

Figure 2. c-Fos–deficient and RANKL-deficient mice show elevated HSPC pools. (A–F) 250 µg/kg/d G-CSF or control PBS was injected subcutaneously into 8–12-wk-old c-Fos-deficient (c-Fos KO; $n = 5$ for each group) or RANKL-deficient (RANKL KO; $n = 5$ for each group) mice or into respective control littermates (wild-type [WT]; $n = 5$ for each group) daily for 5 d. Peripheral blood was collected, and the proportion of HSCs (A, B, D, and E) and CFU-C (C and F) were analyzed. (A and D) Representative flow cytometry pattern of peripheral blood. Cells were gated on lineage-negative cells. Data represent the mean LSK frequency (%) ± SD in peripheral blood (*, $P < 0.01$, $n = 5$ for each group; B and E) and mean CFU-C ± SD in 1 ml peripheral blood (*, $P < 0.01$, $n = 6$ for each group; C and F). Representative data from one of three independent experiments are shown (A–F).

Published October 17, 2011

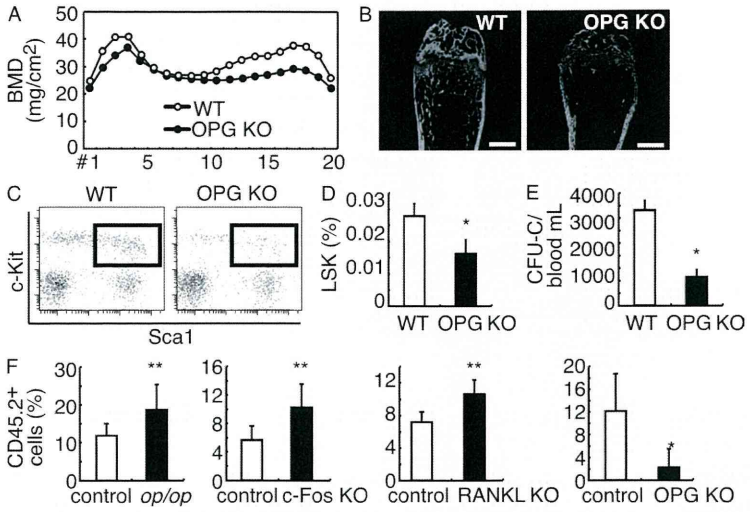

Figure 3. OPG-deficient mice are osteoporotic and have reduced HSPC pools. (A and B) BMD assays and microradiography analysis were undertaken in femurs of 8–12-wk-old OPG-deficient (OPG KO; $n = 5$) and wild-type (WT; $n = 5$) mice using dual-energy x-ray absorptiometry (mg/cm^2; A) and micro-CT (B), respectively. BMD was shown in 20 longitudinal divisions of femurs. Bars, 1 mm. (C–E) 250 µg/kg/d G-CSF was injected subcutaneously into OPG-deficient (OPG KO; $n = 5$) and wild-type control (WT; $n = 5$) mice daily for 5 d. Peripheral blood was then collected, and the frequency of the LSK fraction (C and D) and CFU-C (E) were analyzed by flow cytometry and colony-forming assays, respectively. (C) Representative flow cytometry pattern of peripheral blood cells. Cells were gated with lineage-negative cells. Data represent the mean LSK frequency (%) ± SD in peripheral blood (*, $P < 0.01$, $n = 5$; D) and CFU-C ± SD in 1 ml peripheral blood (*, $P < 0.01$, $n = 12$; E). (F) 250 µg/kg/d G-CSF was injected subcutaneously into OPG-deficient (OPG KO), c-Fos–deficient (c-Fos KO), RANKL-deficient (RANKL KO), and littermate control mice daily for 5 d. Peripheral blood was collected from each mouse and transplanted into lethally irradiated Ly5.1 recipient mice with BM competitors isolated from Ly5.1 mice. Peripheral blood of recipient mice was collected after 3 mo of transplantation and stained with PE-conjugated anti-CD45.1 and FITC-conjugated anti-CD45.2, and leukocyte chimerism was determined by FACS. Data represent the mean CD45.2$^+$ frequency (%) ± SD in peripheral blood (*, $P < 0.01$; **, $P < 0.05$, $n = 8$). Representative data of two (A, B, and F) and three (C, D, and E) independent experiments are shown.

HSPCs was observed in CD11b$^+$ myeloid, B220$^+$ B cell, and CD3$^+$ T cell recipient lineages (Fig. S2). Thus, osteoclasts and BM cavities appear to antagonize HSC maintenance.

F4/80$^+$ osteomacs are defective in *op/op* mice but appear normal in c-Fos– or OPG-deficient mice

Recently, it was reported that F4/80$^+$ macrophages, termed osteomacs, reside in the endosteal (Chang et al., 2008) where they support osteoblast function, thereby contributing to retain HSCs in the BM niche (Winkler et al., 2010). Thus, increased HSPC mobilization seen in *op/op* mice after G-CSF injection could be a result of reduced levels of osteomacs. Indeed, we observed fewer F4/80$^+$ osteomacs in *op/op* mice, although their levels in c-Fos–deficient and RANKL-deficient mice were similar to those observed in wild-type mice (Fig. 4). These observations suggest that osteomac reduction is not a common property of osteopetrotic mice, all of which show increased HSPC mobilization after G-CSF administration. CD11b$^+$F4/80$^+$Ly6-G$^+$ macrophages, which also reportedly inhibit HSPC mobilization into the peripheral blood, are reduced after G-CSF treatment in wild-type mice (Winkler et al., 2010). However, like osteomacs, the CD11b$^+$F4/80$^+$Ly6-G$^+$ macrophage population was reduced in *op/op* mice compared with wild-type mice, but such a reduction was not seen in c-Fos–deficient mice (Fig. S3 A). In OPG-deficient mice, osteomac and CD11b$^+$F4/80$^+$Ly6-G$^+$ macrophage levels were similar to those seen in wild-type mice (Fig. 4 and Fig. S3 A). These results suggest that both of these cell types are M-CSF dependent and are deficient in the *op/op* model of osteopetrotic mice, but that this deficiency is not likely be the cause of increased mobilization of HSPCs seen in osteopetrotic animals. A more likely explanation is that HSPC mobilization seen in all osteopetrotic models is a result of loss of osteoclasts and BM cavities. Because F4/80$^+$ osteomacs and CD11b$^+$F4/80$^+$Ly6-G$^+$ macrophages were detected in osteoclast-deficient c-Fos–deficient mice, we do not consider F4/80$^+$ cells to be osteoclasts. Indeed, F4/80 is reportedly not expressed in osteoclasts (Quinn et al., 1999).

The spleen is not the primary tissue that maintains HSPCs in *op/op* mice

Hematopoiesis in osteopetrotic mice reportedly occurs in extramedullary spaces, such as spleen (Lowell et al., 1996). Indeed, a greater proportion of LSK cells was seen in the

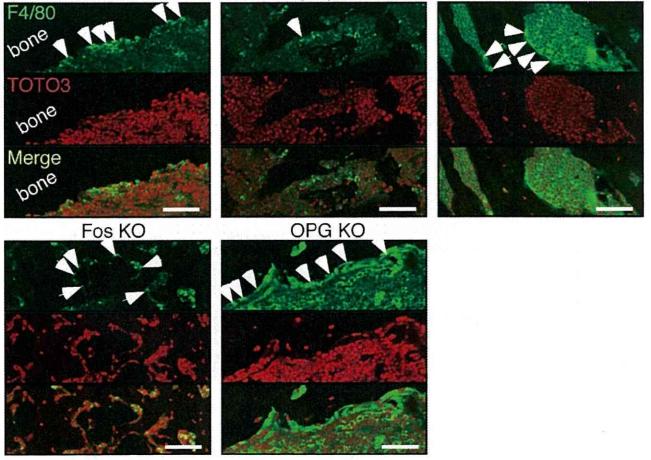

Figure 4. Osteomac levels are reduced in *op/op* but not c-Fos–deficient mice. Paraffin specimens of *op/op*, c-Fos-deficient (c-Fos KO), RANKL-deficient (RANKL KO), OPG-deficient (OPG KO), and control mouse femoral bones were stained with Alexa Fluor 488–conjugated anti-F4/80 antibody and observed under a confocal microscope. TOTO3 served as a nuclear stain. Arrowheads indicate F4/80-positive osteomacs. Representative data of three independent experiments are shown. Bars, 100 µm.

Published October 17, 2011

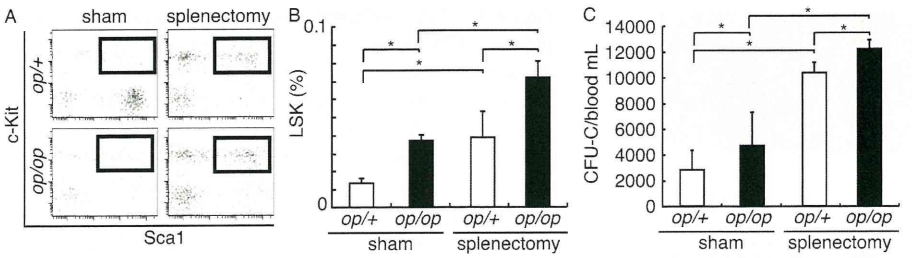

Figure 5. HSCs do not accumulate in the spleen of *op/op* mice. Splenectomy or sham surgery was performed on 8–12-wk-old *op/op* ($n = 5$ for each group) and control (*op/+*; $n = 5$ for each group) mice. 7 d later, mice were injected with 250 µg/kg/d G-CSF daily for 5 d, and mobilization of HSCs to peripheral blood was analyzed using flow cytometry and colony-forming assays. (A) Representative flow cytometry pattern of peripheral blood after G-CSF injection ($n = 5$ for each group). Cells were gated on lineage-negative cells. (B and C) Data represent the mean LSK frequency (%) ± SD in peripheral blood (*, $P < 0.01$, $n = 5$ for each group; B) and mean CFU-C ± SD in 1 ml peripheral blood (*, $P < 0.01$, $n = 5$ for each group; C). Representative data of three independent experiments are shown.

spleen of *op/op* mice than in control (*op/+*) mice (Fig. S3, B and C). Thus, we removed the spleen from *op/op* mice and treated those mice with G-CSF serially to analyze HSPC mobilization (Fig. 5). Interestingly, HSPC mobilization was induced or even significantly higher in splenectomized *op/op* mice compared with sham-operated *op/op* mice (Fig. 5). These data suggest that HSCs are maintained in tissues other than spleen in osteoclast-deficient osteopetrotic mice. Interestingly, we found that bone tissues in osteoclast-deficient mice contained small spaces where c-Kit–positive hematopoietic cells are located (Fig. S4 A). Thus, hematopoiesis may be maintained in bone, even in osteopetrotic mice. In fact, flow cytometry analysis revealed an HSC-enriched LSK population in osteopetrotic bones of *op/op* mice (Fig. S4 B), and these cells were shown to be functional by an LTC-IC assay (not depicted). These results indicate that HSCs are maintained in bones of osteopetrotic mice, that increased bone mass as a result of impaired osteoclastogenesis may increase functionality of the HSC niche, and that osteoclasts could be a therapeutic target to expand HSCs as well as bone mass. Bones are formed by osteoblasts, and osteoblasts reportedly express various niche factors such as angiopoietin 1, osteopontin, Cxcl12, and KitL (Arai et al., 2004; Stier et al., 2005; Adams and Scadden, 2006; Katayama et al., 2006). We found that these niche factors were expressed in osteopetrotic bones of *op/op*, c-Fos–deficient, and RANKL-deficient mice (unpublished data).

Osteoclast-inhibiting agents increase HSPC mobilization in wild-type mice

Finally, we asked whether blocking osteoclast function or differentiation pharmacologically would inhibit or enhance hematopoietic activity in wild-type mice. Wild-type mice were pretreated with bisphosphonate (alendronate) or vehicle (PBS), and HSPC mobilization after serial G-CSF injection was analyzed (Fig. 6). Bisphosphonate treatment significantly increased bone mass (Fig. 6, A and B), and, interestingly, mobilization of HSPCs as determined by a colony-forming assay was highly induced in bisphosphonate- compared with vehicle-treated mice (Fig. 6 C). Thus, bisphosphonate therapy increased bone mass and up-regulated HSPC mobilization. Similar phenotypes were detected in mice treated with neutralizing RANKL antibody compared with isotype-matched control antibody-treated mice (Fig. 6, D–F). Thus our results demonstrate that HSCs can be expanded pharmacologically. Treatment with zoledronate, another bisphosphonate, also reportedly increased HSPC mobilization in response to G-CSF (Winkler et al., 2010), further suggesting that bisphosphonate, neutralizing RANKL antibody, or other osteoclast inhibitors might serve as adjuvants to increase HSPC mobilization.

Collectively, our results challenge the dogma that BM cavity–deficient animals cannot maintain HSCs and raises the question of why mammalian and avian species developed BM cavities. Although the density of osteopetrotic bones in *op/op* mice was greater than that seen in controls (Fig. S5 A), strength

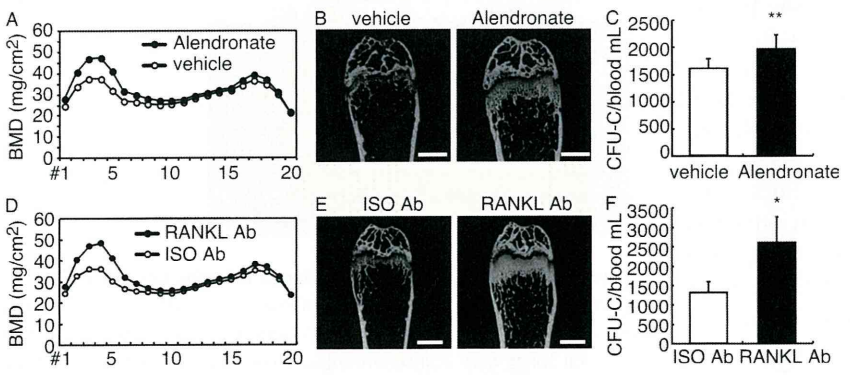

Figure 6. Pharmacological inhibition of osteoclasts increases bone mass and expands the HSC pool in wild-type mice. (A–C) Wild-type mice were treated with 5 mg per mouse of alendronate (bisphosphonate; $n = 5$) or vehicle (PBS; $n = 5$) daily for 14 d and then injected with 250 µg/kg/d G-CSF daily for five more days. Mice were assessed for BMD (A), microradiography (B), and HSC mobilization in peripheral blood (C; **, $P < 0.05$, $n = 5$). Bar, 1 mm. (D and E) Wild-type mice were treated with 5 or 2.5 mg/kg of neutralizing antibody against RANKL (RANKL Ab; $n = 5$) or isotype control antibody (ISO; $n = 5$) 14 and 1 d before G-CSF injection, respectively. Mice were then injected with 250 µg/kg/d G-CSF daily for 5 d, and BMD (D), microradiography (E), and mobilization of HSCs in peripheral blood (F; *, $P < 0.01$, $n = 5$) were analyzed. BMD was shown in 20 longitudinal divisions of femurs (A and D). Data represent mean CFU-C ± SD in 1 ml peripheral blood (C and F). Bars, 1 mm. Representative data of two independent experiments are shown.

Published October 17, 2011

tests indicated that bones were more fragile than control bones (Fig. S5 B). Fractures were induced in osteopetrotic bones earlier and by lower energy than in control bones, based on constant displacement tests (Fig. S5, B and C). Osteopetrotic bone also showed reduced elasticity (Fig. S5 D). H/E staining indicated that *op/op* mouse bones were filled with trabecular bone and that mutants exhibited thinner cortical bones than did control mice (Fig. S5, E and F). Indeed, osteopetrotic patients suffer from frequent fractures (Landa et al., 2007). Thus bones likely developed not only to maintain HSCs but to optimize bone strength and body support. To overcome the reduced ability to support HSCs in an open BM cavity created by osteoclasts, BM niches were likely developed by osteoblastic cells, vascular endothelial cells, reticular cells, or aggregates of these cells (Adams and Scadden, 2006; Kiel and Morrison, 2008), or by the products of these cells such as angiopoietin 1, osteopontin, Cxcl12, and thrombopoietin 1 (Calvi et al., 2003; Zhang et al., 2003; Arai et al., 2004; Kiel et al., 2005; Stier et al., 2005; Adams and Scadden, 2006; Sugiyama et al., 2006; Kiel and Morrison, 2008; Lymperi et al., 2010).

Manipulating HSCs in vitro to increase their number likely results in reduced stemness because quiescence is essential to maintain stem cell function (Cheng et al., 2000; Miyamoto et al., 2007). Thus, there is likely an antagonistic relationship between expansion and quiescence in HSC expansion. Bone mineral density (BMD) decreases with age, as osteoporosis is increased by osteoclastic activity (Manolagas and Jilka, 1995; Teitelbaum, 2007). Hematopoietic activity also decreases with age (Geiger and Rudolph, 2009; Waterstrat and Van Zant, 2009), suggesting that bone aging can cause both reduced bone mass and reduced hematopoiesis, and that antagonizing osteoclasts pharmacologically could promote increased bone mass and stimulate an induced niche in vivo to increase the HSC pool.

MATERIALS AND METHODS

Mice. *op/op*, c-Fos–deficient, and RANKL-deficient mice were generated by crossing heterozygotes of respective genotypes. c-Fos-deficient mice were provided by E. Wagner (Institute of Molecular Biotechnology of the Austrian Academy of Sciences, Vienna, Austria). Animals were maintained under pathogen-free conditions in animal facilities certified by the Keio University School of Medicine animal care committee. To analyze blood counts, peripheral blood from the postorbital vein was collected in heparinized microtubes (Drummond Scientific). 5-FU (Kyowa Hakko Kirinn) was administered intravenously at 150 mg/kg to 8–12-wk-old *op/op*, c-Fos–deficient, or littermate control mice once a week, and mouse survival was monitored daily. Animal protocols were approved by the Keio University School of Medicine animal care committee.

Analysis of skeletal morphology. 8–12-wk-old mice were necropsied, and their hindlimbs were removed, fixed in 70% ethanol, and subjected to dual energy x-ray absorptiometry analysis to measure BMD and for microradiographic analysis. BMD was shown in 20 longitudinal divisions of femurs.

Mobilization of hematopoietic progenitors. To induce HSPC mobilization, mice were injected with recombinant human G-CSF (Kyowa Hakko Kirin Co.; 250 μg/kg/d for 5 d, subcutaneous injection). Peripheral blood was harvested 3 h after the last G-CSF injection and used for blood counts, determination of colony-forming units in culture (CFU-C), and flow cytometric (FACS) analysis. Blood counts were analyzed using CellTac (Nihon Kohden). For CFU-C assays, cells were cultured in methylcellulose medium containing recombinant mouse (rm) stem cell factor, rm IL-3, recombinant human (rh) IL-6, and rh erythropoietin (MethoCult GF M3434; STEMCELL Technologies) in 35-mm culture dishes (Falcon) and incubated at 37°C in 5% CO_2. The number of CFU-Cs was determined on day 7 using a microscope (Olympus). FACS analysis was undertaken as described. For some experiments, Alendronate or RANKL neutralizing antibody was administered. 5 μg alendronate/mouse/d was injected subcutaneously for 14 d before G-CSF injection. 5 mg/kg RANKL neutralizing antibody (Oriental Yeast Co.) or isotype control antibody (BD) at 14 d and 2.5 mg/kg at 1 d before G-CSF injection was injected into the peritoneal cavity. For competitive repopulation assays, peripheral blood from individual $CD45.2^+$ mice was pooled, and 20 μl of pooled blood was mixed with 500,000 competitive BM cells from untreated $CD45.1^+$ mice and injected intravenously into lethally irradiated $CD45.1^+$ recipient mice. After 3 mo of transplantation, peripheral blood reconstitution in multiple lineages was determined by FACS using CD45.1 (A20), CD45.2 (104), Mac1 (M1/70), CD3 (500A2), and B220 (RA3-6B2) antibodies (all BD).

Flow cytometry. mAbs (all BD) recognizing the following markers were used for flow cytometric analyses and cell sorting: c-Kit (2B8), Sca-1 (E13-161.7), CD3 (500A2) B220 (RA3-6B2), TER-119 (Ly-76), Gr-1 (RB6-8C5), and Mac-1 (M1/70). A mixture of mAbs recognizing CD3, B220, TER-119, Mac-1, or Gr-1 was used to identify $lineage^+$ cells. Mature myeloid cells were stained with PEcy7-conjugated anti-CD11b (M1/70; eBioscience), Alexa Fluor 488–conjugated anti-F4/80 (CI:A3-1; BioLegend), and PE-conjugated anti–Ly6-G antibody (1A8; BD). Stained cells were analyzed on a FACS Aria2 machine (BD).

ELISA. Serum M-CSF levels were assayed using the Mouse M-CSF ELISA kit (R&D Systems), according to the manufacturer's instructions.

Immunohistochemical analysis. Frozen sections of *op/op* mice femoral bone that had not been decalcified were stained with goat anti–c-Kit antibody (AF1356; R&D Systems), followed by Alexa Fluor 488–conjugated donkey anti–goat antibody (Invitrogen) to detect HSCs and with TOTO3 (Invitrogen) to detect nuclei. Samples were observed under a fluorescence microscope (IX70; Olympus). Paraffin sections of wild-type, *op/op*, c-Fos–deficient, and OPG-deficient mice femoral bone were stained with Alexa Fluor 488–conjugated anti-F4/80 antibody (BioLegend) and TOTO3 as a nuclear stain and then observed under a confocal microscope (FV1000; Olympus).

Bone strength test. The femur was removed from mice and placed on the lower supports of a three point bending fixture with the anterior side facing up using an apparatus called the Bone Strength Tester MZ-500S (Maruto) installed with a load of 50 N. The span between the two lower supports was set at 6 mm. For all femoral specimens, the upper loading device was aligned to the center of the femoral shaft and the load was applied at a constant displacement rate of 10 mm/min until breakage occurred.

Online supplemental material. Fig. S1 demonstrates the sensitivity of c-Fos–deficient and *op/op* mice to 5-FU, and the bone phenotype of RANKL-deficient mice. Fig. S2 shows multilineage reconstitution of donor-derived cells in recipient mice. Fig. S3 demonstrates the frequency of the $CD11b^+F4/80^+Ly6\text{-}G^+$ macrophage population in wild-type, *op/op*, c-Fos–deficient, and OPG-deficient mice, and the frequency of LSK cells in *op/op* mouse spleen. Fig. S4 demonstrates the presence of HSCs in osteopetrotic bone. Fig. S5 shows osteopetrotic bone strength. Online supplemental material is available at http://www.jem.org/cgi/content/full/jem.20101890/DC1.

We thank Professor Wagner for providing c-Fos–deficient mice and Drs. Momoshima, Ishikawa, and Mogoe, Mr. Yamazaki, and Mrs. K. Fukushima for technical support.

K. Miyamoto was supported by a grant-in-aid for Young Scientists (B). T. Miyamoto was supported by a grant-in-aid for Young Scientists (A) and by Precursory Research for Embryonic Science and Technology (PREST), the Takeda Science Foundation, the Nakatomi Foundation, the Inamori Foundation, and the Keio Kanrinmaru project, Japan.

The authors have no conflicting financial interests.

Submitted: 9 September 2010
Accepted: 22 September 2011

Published October 17, 2011

REFERENCES

Adams, G.B., and D.T. Scadden. 2006. The hematopoietic stem cell in its place. *Nat. Immunol.* 7:333–337 . http://dx.doi.org/10.1038/ni1331

Arai, F., A. Hirao, M. Ohmura, H. Sato, S. Matsuoka, K. Takubo, K. Ito, G.Y. Koh, and T. Suda. 2004. Tie2/angiopoietin-1 signaling regulates hematopoietic stem cell quiescence in the bone marrow niche. *Cell.* 118: 149–161. http://dx.doi.org/10.1016/j.cell.2004.07.004

Bucay, N., I. Sarosi, C.R. Dunstan, S. Morony, J. Tarpley, C. Capparelli, S. Scully, H.L. Tan, W. Xu, D.L. Lacey, et al. 1998. osteoprotegerin-deficient mice develop early onset osteoporosis and arterial calcification. *Genes Dev.* 12:1260–1268. http://dx.doi.org/10.1101/gad.12.9.1260

Calvi, L.M., G.B. Adams, K.W. Weibrecht, J.M. Weber, D.P. Olson, M.C. Knight, R.P. Martin, E. Schipani, P. Divieti, F.R. Bringhurst, et al. 2003. Osteoblastic cells regulate the haematopoietic stem cell niche. *Nature.* 425:841–846. http://dx.doi.org/10.1038/nature02040

Chang, M.K., L.J. Raggatt, K.A. Alexander, J.S. Kuliwaba, N.L. Fazzalari, K. Schroder, E.R. Maylin, V.M. Ripoll, D.A. Hume, and A.R. Pettit. 2008. Osteal tissue macrophages are intercalated throughout human and mouse bone lining tissues and regulate osteoblast function in vitro and in vivo. *J. Immunol.* 181:1232–1244.

Cheng, T., N. Rodrigues, H. Shen, Y. Yang, D. Dombkowski, M. Sykes, and D.T. Scadden. 2000. Hematopoietic stem cell quiescence maintained by p21cip1/waf1. *Science.* 287:1804–1808. http://dx.doi.org/10.1126/science.287.5459.1804

Chitu, V., and E.R. Stanley. 2006. Colony-stimulating factor-1 in immunity and inflammation. *Curr. Opin. Immunol.* 18:39–48. http://dx.doi.org/10.1016/j.coi.2005.11.006

Christopher, M.J., and D.C. Link. 2008. Granulocyte colony-stimulating factor induces osteoblast apoptosis and inhibits osteoblast differentiation. *J. Bone Miner. Res.* 23:1765–1774. http://dx.doi.org/10.1359/jbmr.080612

Freedman, M.H., and E.F. Saunders. 1981. Hematopoiesis in the human spleen. *Am. J. Hematol.* 11:271–275. http://dx.doi.org/10.1002/ajh.2830110307

Geiger, H., and K.L. Rudolph. 2009. Aging in the lympho-hematopoietic stem cell compartment. *Trends Immunol.* 30:360–365. http://dx.doi.org/10.1016/j.it.2009.03.010

Grigoriadis, A.E., Z.Q. Wang, M.G. Cecchini, W. Hofstetter, R. Felix, H.A. Fleisch, and E.F. Wagner. 1994. c-Fos: a key regulator of osteoclast-macrophage lineage determination and bone remodeling. *Science.* 266: 443–448. http://dx.doi.org/10.1126/science.7939685

Heissig, B., K. Hattori, S. Dias, M. Friedrich, B. Ferris, N.R. Hackett, R.G. Crystal, P. Besmer, D. Lyden, M.A. Moore, et al. 2002. Recruitment of stem and progenitor cells from the bone marrow niche requires MMP-9 mediated release of kit-ligand. *Cell.* 109:625–637. http://dx.doi.org/10.1016/S0092-8674(02)00754-7

Katayama, Y., M. Battista, W.M. Kao, A. Hidalgo, A.J. Peired, S.A. Thomas, and P.S. Frenette. 2006. Signals from the sympathetic nervous system regulate hematopoietic stem cell egress from bone marrow. *Cell.* 124:407–421. http://dx.doi.org/10.1016/j.cell.2005.10.041

Kiel, M.J., and S.J. Morrison. 2008. Uncertainty in the niches that maintain haematopoietic stem cells. *Nat. Rev. Immunol.* 8:290–301. http://dx.doi.org/10.1038/nri2279

Kiel, M.J., O.H. Yilmaz, T. Iwashita, O.H. Yilmaz, C. Terhorst, and S.J. Morrison. 2005. SLAM family receptors distinguish hematopoietic stem and progenitor cells and reveal endothelial niches for stem cells. *Cell.* 121: 1109–1121. http://dx.doi.org/10.1016/j.cell.2005.05.026

Kollet, O., A. Dar, S. Shivtiel, A. Kalinkovich, K. Lapid, Y. Sztainberg, M. Tesio, R.M. Samstein, P. Goichberg, A. Spiegel, et al. 2006. Osteoclasts degrade endosteal components and promote mobilization of hematopoietic progenitor cells. *Nat. Med.* 12:657–664. http://dx.doi.org/10.1038/nm1417

Kong, Y.Y., H. Yoshida, I. Sarosi, H.L. Tan, E. Timms, C. Capparelli, S. Morony, A.J. Oliveira-dos-Santos, G. Van, A. Itie, et al. 1999. OPGL is a key regulator of osteoclastogenesis, lymphocyte development and lymph-node organogenesis. *Nature.* 397:315–323. http://dx.doi.org/10.1038/16852

Landa, J., N. Margolis, and P. Di Cesare. 2007. Orthopaedic management of the patient with osteopetrosis. *J. Am. Acad. Orthop. Surg.* 15:654–662.

Lowell, C.A., M. Niwa, P. Soriano, and H.E. Varmus. 1996. Deficiency of the Hck and Src tyrosine kinases results in extreme levels of extramedullary hematopoiesis. *Blood.* 87:1780–1792.

Lymperi, S., F. Ferraro, and D.T. Scadden. 2010. The HSC niche concept has turned 31. Has our knowledge matured? *Ann. N. Y. Acad. Sci.* 1192:12–18. http://dx.doi.org/10.1111/j.1749-6632.2009.05223.x

Manolagas, S.C., and R.L. Jilka. 1995. Bone marrow, cytokines, and bone remodeling. Emerging insights into the pathophysiology of osteoporosis. *N. Engl. J. Med.* 332:305–311. http://dx.doi.org/10.1056/NEJM199502023320506

Miyamoto, K., K.Y. Araki, K. Naka, F. Arai, K. Takubo, S. Yamazaki, S. Matsuoka, T. Miyamoto, K. Ito, M. Ohmura, et al. 2007. Foxo3a is essential for maintenance of the hematopoietic stem cell pool. *Cell Stem Cell.* 1:101–112. http://dx.doi.org/10.1016/j.stem.2007.02.001

Miyamoto, T., O. Ohneda, F. Arai, K. Iwamoto, S. Okada, K. Takagi, D.M. Anderson, and T. Suda. 2001. Bifurcation of osteoclasts and dendritic cells from common progenitors. *Blood.* 98:2544–2554. http://dx.doi.org/10.1182/blood.V98.8.2544

Mizuno, A., N. Amizuka, K. Irie, A. Murakami, N. Fujise, T. Kanno, Y. Sato, N. Nakagawa, H. Yasuda, S. Mochizuki, et al. 1998. Severe osteoporosis in mice lacking osteoclastogenesis inhibitory factor/osteoprotegerin. *Biochem. Biophys. Res. Commun.* 247:610–615. http://dx.doi.org/10.1006/bbrc.1998.8697

Quinn, J.M., M. Morfis, M.H. Lam, J. Elliott, V. Kartsogiannis, E.D. Williams, M.T. Gillespie, T.J. Martin, and P.M. Sexton. 1999. Calcitonin receptor antibodies in the identification of osteoclasts. *Bone.* 25:1–8. http://dx.doi.org/10.1016/S8756-3282(99)00094-0

Stier, S., Y. Ko, R. Forkert, C. Lutz, T. Neuhaus, E. Grünewald, T. Cheng, D. Dombkowski, L.M. Calvi, S.R. Rittling, and D.T. Scadden. 2005. Osteopontin is a hematopoietic stem cell niche component that negatively regulates stem cell pool size. *J. Exp. Med.* 201:1781–1791. http://dx.doi.org/10.1084/jem.20041992

Sugiyama, T., H. Kohara, M. Noda, and T. Nagasawa. 2006. Maintenance of the hematopoietic stem cell pool by CXCL12-CXCR4 chemokine signaling in bone marrow stromal cell niches. *Immunity.* 25:977–988. http://dx.doi.org/10.1016/j.immuni.2006.10.016

Takamatsu, Y., P.J. Simmons, R.J. Moore, H.A. Morris, L.B. To, and J.P. Lévesque. 1998. Osteoclast-mediated bone resorption is stimulated during short-term administration of granulocyte colony-stimulating factor but is not responsible for hematopoietic progenitor cell mobilization. *Blood.* 92:3465–3473.

Teitelbaum, S.L. 2007. Osteoclasts: what do they do and how do they do it? *Am. J. Pathol.* 170:427–435. http://dx.doi.org/10.2353/ajpath.2007.060834

Watanabe, T., H. Suzuya, T. Onishi, S. Kanai, M. Kaneko, H. Watanabe, R. Nakagawa, Y. Kawano, Y. Takaue, Y. Kuroda, and J.E. Talmadge. 2003. Effect of granulocyte colony-stimulating factor on bone metabolism during peripheral blood stem cell mobilization. *Int. J. Hematol.* 77:75–81. http://dx.doi.org/10.1007/BF02982606

Waterstrat, A., and G. Van Zant. 2009. Effects of aging on hematopoietic stem and progenitor cells. *Curr. Opin. Immunol.* 21:408–413. http://dx.doi.org/10.1016/j.coi.2009.05.002

Winkler, I.G., N.A. Sims, A.R. Pettit, V. Barbier, B. Nowlan, F. Helwani, I.J. Poulton, N. van Rooijen, K.A. Alexander, L.J. Raggatt, and J.P. Lévesque. 2010. Bone marrow macrophages maintain hematopoietic stem cell (HSC) niches and their depletion mobilizes HSCs. *Blood.* 116: 4815–4828. http://dx.doi.org/10.1182/blood-2009-11-253534

Yoshida, H., S. Hayashi, T. Kunisada, M. Ogawa, S. Nishikawa, H. Okamura, T. Sudo, L.D. Shultz, and S. Nishikawa. 1990. The murine mutation osteopetrosis is in the coding region of the macrophage colony stimulating factor gene. *Nature.* 345:442–444. http://dx.doi.org/10.1038/345442a0

Zhang, J., C. Niu, L. Ye, H. Huang, X. He, W.G. Tong, J. Ross, J. Haug, T. Johnson, J.Q. Feng, et al. 2003. Identification of the haematopoietic stem cell niche and control of the niche size. *Nature.* 425:836–841. http://dx.doi.org/10.1038/nature02041

J Orthop Sci (2011) 16:785–790
DOI 10.1007/s00776-011-0135-2

ORIGINAL ARTICLE

Matrix metalloproteinase 13 in the ligamentum flavum from lumbar spinal canal stenosis patients with and without diabetes mellitus

Guanyu Cui · Kota Watanabe · Yoshiteru Miyauchi · Naobumi Hosogane · Takashi Tsuji · Ken Ishii · Masaya Nakamura · Yoshiaki Toyama · Kazuhiro Chiba · Takeshi Miyamoto · Morio Matsumoto

Received: 2 March 2011 / Accepted: 12 July 2011 / Published online: 10 August 2011

Abstract
Background Lumbar spinal canal stenosis (LSCS) is one of the most common spinal disorders in the elderly, and ligamentum flavum (LF) hypertrophy is an important cause of LSCS. Matrix metalloproteinase 13 (MMP13) can degrade fibrillar collagens and elastic microfibrils, and is involved in inflammation and fibrosis. The purpose of this study was to compare the expression of MMP13 in the LF from LSCS patients with diabetes mellitus [DM (+)] with that in the LF from patients without DM [DM (−)] and to analyze the relationship among DM, MMP13 expression, and LF hypertrophy.
Methods LFs from 11 DM (+) and 24 DM (−) LSCS patients were analyzed in this study. Histology analysis using hematoxylin and eosin and Masson's trichrome stain was performed for each LF. The expression of MMP13 was analyzed by quantitative real-time PCR. The thickness of LF was measured by CT.
Results In the LF from DM (+) LSCS patients, the elastic fibers were more disorganized and had lower volumes than in the LF from DM (−) LSCS patients, while more fibrotic tissue was observed in the LF from DM (+) than from DM (−) LSCS patients. MMP13 expression was significantly higher in the LF from DM (+) LSCS patients (0.46 ± 0.61 vs. 0.05 ± 0.09, $P = 0.002$). The LF from the DM (+) LSCS patients was significantly thicker than that from the DM (−) LSCS patients (5.0 ± 0.9 vs. 3.1 ± 0.8 mm, $P < 0.01$), and the thickness was correlated with the expression of MMP13 (correlation coefficient = 0.43, $P = 0.01$, Pearson's correlation test).
Conclusion DM-related MMP13 expression can be one of the factors contributing to fibrosis and hypertrophy of the LF. Further research on the mechanism of this process may lead to new therapies for LF hypertrophy.

G. Cui · Y. Miyauchi · N. Hosogane · T. Tsuji · K. Ishii · M. Nakamura · Y. Toyama · K. Chiba · T. Miyamoto · M. Matsumoto (✉)
Department of Orthopedic Surgery, Keio University School of Medicine, 35 Shinanomachi, Shinjuku, Tokyo 160-8582, Japan
e-mail: morio@sc.itc.keio.ac.jp

G. Cui
Department of Spinal Surgery, Beijing Jishuitan Hospital, Peking University, Beijing, People's Republic of China

K. Watanabe
Department of Advanced Therapy for Spine and Spinal Cord Disorders, Keio University School of Medicine, Tokyo, Japan

Introduction

Lumbar spinal canal stenosis (LSCS) is one of the most common spinal disorders in the elderly. The causes of LSCS include ligamentum flavum (LF) hypertrophy, hypertrophy of the facet joints, bulging of the intervertebral discs, and vertebral endplate osteophytosis. Among them, LF hypertrophy plays a dominant role in the narrowing of the lumbar spinal canal [1]. In the lower lumbar spine, the LF is composed of thick elastic fibers that are densely arranged with interspersed collagen fibers [2]. Histological changes in the hypertrophied LF from LSCS patients include fibrosis, degradation of elastic fibers with an increase in collagen fibers, granulation tissue proliferation, chondroid metaplasia, and calcification [3–6]. Fibrosis is considered to be the main cause of LF hypertrophy, and transforming growth factor (TGF)-β released by endothelial cells may stimulate the fibrosis, especially during the early phase of hypertrophy [3]. However, the pathomechanism of LF hypertrophy remains unclear.

The matrix metalloproteinases (MMPs) include over 20 zinc-dependent enzymes that degrade or modify

extracellular matrix molecules, such as elastin, collagen, and proteoglycans [7, 8]. Several recent studies have demonstrated a role of MMP3 [9] or MMP inhibitors in the pathology of LF [10].

Of the MMPS, MMP13 can degrade fibrillar collagens, including type I, II, and III collagens, into gelatin. It can also degrade the elastic microfibrils that are involved in extracellular matrix remodeling [11]. In addition, MMP13 plays a role in inflammatory and fibrotic processes [12–14]. MMP13 was reported to be more highly expressed in the LF of LSCS patients than in that of disc herniation patients, and is expressed in LF fibroblasts [15]. Moreover, high plasma glucose increases the expression of MMP13 in vessels [16] and the cornea [17].

We hypothesize that diabetes mellitus (DM) can cause an increased expression of MMP13 in the LF, which may lead to fibrosis and extracellular matrix remodeling and finally cause LF hypertrophy. The purpose of this study was to compare the expression of MMP13 in the LF of LSCS patients with DM [DM (+)] with that in the LF of patients without DM [DM (−)] and to analyze the relationship among DM, MMP13 expression, and LF hypertrophy.

Materials and methods

Thirty-five LF samples were obtained from 35 LSCS patients who underwent decompressive laminectomy for neurogenic claudication. The demographic data of the patients are shown in Table 1. All patients gave informed consent to participate in this study, and the study was approved by the Institutional Review Board of our institute. The mean age was 76.7 ± 7.6 years in the DM (+) group and 72.6 ± 7.4 years in the DM (−) group. There was no difference in age or gender between the two groups ($P > 0.05$). CT images of the lumbar spine of 1 mm thickness were made for all the patients before surgery.

Histologic analysis with hematoxylin-eosin staining and Masson's trichrome staining

During surgery, the LF was removed en-bloc, and the epidural fat was detached. Half of each sample was immediately stored in a −80°C freezer for subsequent quantitative real-time PCR analysis; the other half was fixed in 4% neutral formalin and decalcified in 20% ethylenediaminetetraacetic acid (EDTA) for 4 weeks, then embedded in paraffin for histologic analyses. Two consecutive sections (4 μm thick) were cut on a microtome and subjected to hematoxylin-eosin (H&E) and Masson's trichrome staining, respectively. H&E staining was used to analyze the degradation of the elastic fibers, and Masson's trichrome staining was used to determine the degree of fibrosis [18]. Masson's trichrome staining exhibited elastic fibers as pink and collagen fibers as blue in color.

Paraffin sections of yellow ligament were stained with rabbit anti-MMP13 antibody (Abcam, no. ab39012) followed by Alexa488-conjugated goat anti-rabbit antibody (molecular probe) and TOTO3 (molecular probe) as a nuclear stain, and then observed under a confocal microscope (FV1000, Olympus).

Table 1 Demographic data of the patients

	DM (+)	DM (−)
Age (years)	76.7 ± 7.6 (range 67–84)	72.6 ± 7.4 (range 60–88)
Gender	Female 5, male 6	Female 12, male 12
Level	L2/3: 1, L3/4: 2, L4/5: 7, L5/S1: 1	L3/4: 3, L4/5: 20, L5/S1: 1

Quantitative real-time PCR

The total RNAs were isolated from LF samples by TRIzol reagent (Invitrogen Corp.), and the concentration and quality were determined with an ND-1000 spectrophotometer (NanoDrop). The first-strand cDNAs were synthesized using an Advantage RT-for-PCR kit (Clontech Laboratories Inc.), then subjected to real-time PCR analysis using SYBR Premix ExTaq II (Takara Bio Inc.) according to the manufacturer's instructions. The MMP13 mRNA was normalized to the β-actin mRNA in each sample. PCR amplification was carried out on a Thermal Cycler Dice Real-Time System (Takara Bio Inc.), and gene expression was quantified using the delta-delta Ct method [19]. Nucleotide sequences of the primers were as follows: MMP13 forward: 5′-GCCAGAACTTCCCAACCAT-3′, MMP13 reverse: 5′-GGGCCCAGAATTTTCTCC-3′, β-actin forward: 5′-TGAGCGCGGCTACAGCTT-3′, and β-actin reverse: 5′-TCCTTAATGTCACGCACGATTT-3′.

Measurement of LF thickness

The LF thickness was measured using the preoperative axial CT images. The thickness of the LF on both sides was measured at its midpoints at the level of the decompressed intervertebral disc, following the method proposed by Fukuyama et al. [20], using image-analysis software (Real INTAGE, Tokyo, Japan) that allowed digital measurements with a precision of 0.1 mm.

The measurements were repeated five times by the first author (G.C.), and the results were averaged. To assess the intra- and inter-observer reliability of measurements, CT images of LF from 20 patients were chosen in a random fashion and were measured again by the first author

2 weeks after his first measurement and by the second author (K.W.). The intra- and inter-observer reliability were statistically tested using an intraclass correlation coefficient. The data presented in the results section are based on the measurements by the first author.

Real-time PCR for *mmp13*

To evaluate the influence of glucose on mmp13 expression in fibroblasts, which are the main component of the LF, NIH3T3 fibroblastic cells from mice were cultured in serum-free Dulbecco's Modified Eagle's Medium (Sigma-Aldrich) for 24 h. Then cells were treated with or without 3 mg/ml glucose for 19 h. Subsequently, total RNA was isolated from NIH3T3 cells using an RNeasy mini kit (Qiagen, Hilden, Germany). Single-stranded complementary DNAs (cDNAs) were synthesized with reverse transcriptase (Clontech Laboratories, Palo Alto, CA). Real-time PCR was performed using SYBR Premix ExTaq II (Takara Bio Inc., Otsu, Shiga, Japan) with a DICE Thermal Cycler (Takara Bio Inc.), according to the manufacturer's instructions. *β-Actin* expression served as an internal control. Primer sequences were as follows:

mmp13-forward:	5′-AACCTGGACAAGCAGTTCCAAAG-3′
mmp13-reverse:	5′-GAAATGGCTTTTGCCAGTGTAGG-3′
β-actin-forward:	5′-TGAGAGGGAAATCGTGCGTGAC-3′
β-actin-reverse:	5′-AAGAAGGAAGGCTGGAAAAGAG-3′

Statistical analysis

All values were reported as mean ± standard deviation. All data were analyzed with the SPSS system (version 13.0). Comparisons between the two groups were made by the Mann-Whitney *U* test. The relationship between MMP13 expression and LF thickness was analyzed by Pearson's test. $P < 0.05$ indicated statistical significance.

Results

Hematoxylin-eosin staining

In the LF from DM (+) LSCS patients, the elastic fibers were fragmented, disorganized and focally lost, accompanied by a proliferation of collagen fibers (Fig. 1a, b), while, in the LF from DM (−) LSCS patients, rich elastic fibers were arrayed in parallel order (Fig. 1c, d).

Masson's trichrome staining

In the Masson's trichrome staining of the LF from DM (+) patients, a large area was stained blue, indicating the presence of massive fibrosis (Fig. 1e, f), whereas in the LF from DM (−) patients, a large area was stained pink and showed a regular arrangement, indicating a normal, non-fibrotic condition (Fig. 1g, h).

The immunostaining of MMP13 using the rabbit anti-MMP13 antibody exhibited enhanced expression of MMP13 in the LF from DM (+) patients compared with DM (−) patients (Fig. 2).

MMP13 expression measured by quantitative real-time PCR

The ratio of MMP13 to β-actin mRNA was 0.46 ± 0.61 (range 0.0009–1.5801) for the DM (+) group and 0.05 ± 0.09 (range 0.000001–0.403321) for the DM (−) group (Fig. 3). The MMP13 mRNA expression was significantly higher in the LF from the DM (+) patients than in that from the DM (−) patients ($P = 0.002$).

Thickness of the LF

The mean thickness of the LF measured on CT images was 5.0 ± 0.9 mm (range 3.5–6.7 mm) in the DM (+) group and 3.1 ± 0.8 (range 1.9–4.7 mm) in the DM (−) group (Fig. 4). The LF from DM (+) patients was significantly thicker than that from DM (−) patients ($P < 0.01$). For intra-observer reliability of measurements, the intra-class correlation coefficient was 0.991 (95% confidence interval 0.984–0.996). For the inter-observer reliability, it was 0.970 (0.944–984). Thus, both intra- and inter-observer reliability were acceptably high.

Correlation between MMP13 expression and LF thickness

A positive correlation was observed between the MMP13 expression and thickness of the LF both in DM (+) LSCS patients (correlation coefficient = 0.646, $P = 0.032$, Pearson's correlation test) and in DM (−) LSCS patients (correlation coefficient = 0.542, $P = 0.006$, Pearson's correlation test). Thus, the correlation coefficient was higher in DM (+) patients than in DM (−) patients.

mmp13 expression in NIH3T3 cells

mmp13 expression in NIH3T3 cells analyzed by real-time PCR was 1.50 ± 0.06 times higher in the cells cultured with glucose than in those cultured without ($P < 0.001$) (Fig. 5).

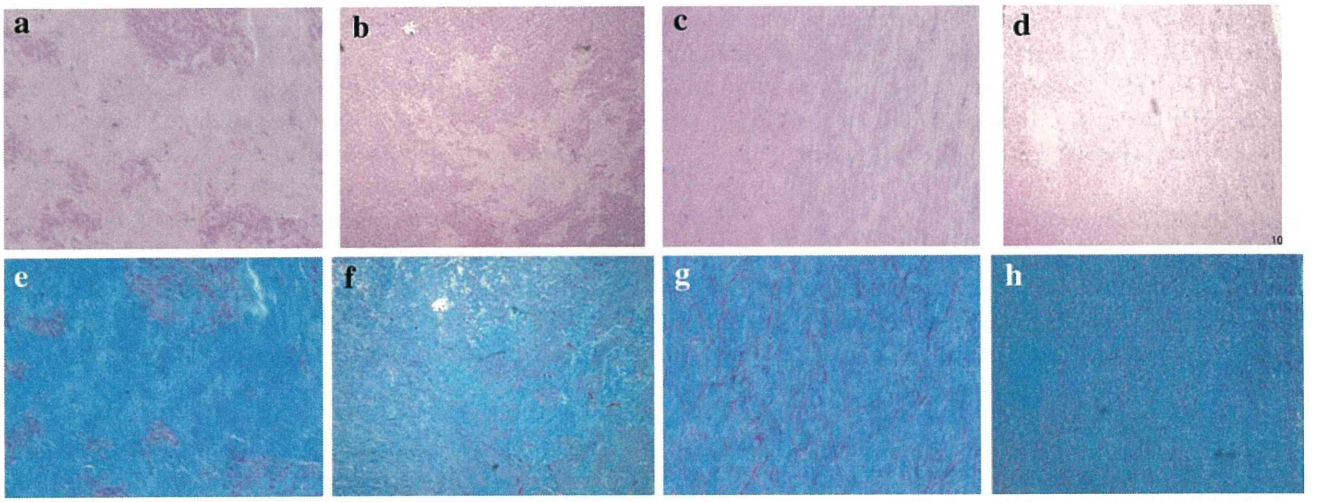

Fig. 1 **a** In the LF from DM (+) LSCS patients, elastic fibers were disorganized and focally lost, accompanied by a proliferation of collagen fibers. The elastic fibers also had low volumes and uneven diameters. H&E staining ×200. **b** LF from DM (+) LSCS patients. H&E staining ×40. **c** In the LF from DM (−) LSCS patients, a large area was stained pink with a regular arrangement, indicating a normal, non-fibrotic condition. H&E staining ×200. **d** LF from DM (−) LSCS patients. H&E staining ×40. **e** In the LF from DM (+) LSCS patients, a large area was stained blue, indicating the presence of massive fibrosis. Masson's trichrome staining ×200. **f** LF from DM (+) LSCS patients. Masson's trichrome staining ×40. **g** In the LF from DM (−) LSCS patients, rich elastic fibers were regularly arrayed, and the diameters of the elastic fibers varied only slightly. Masson's trichrome staining ×200. **h** LF from DM (−) LSCS patients. Masson's trichrome staining ×40

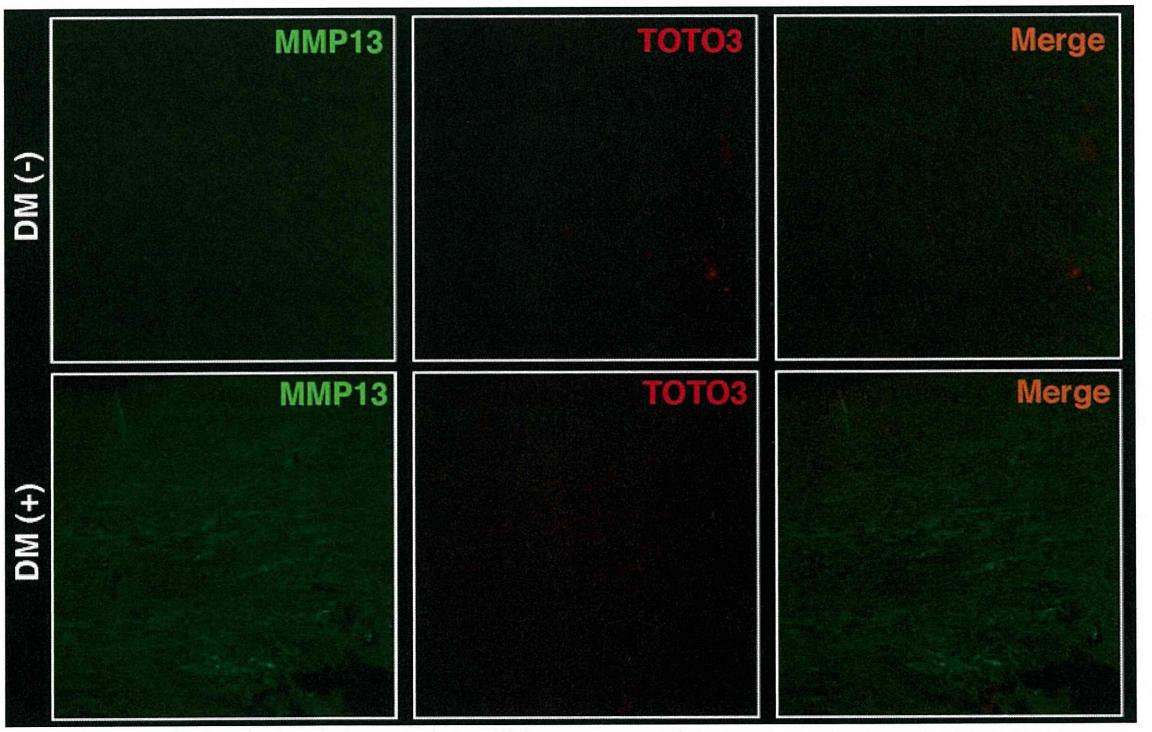

Fig. 2 Paraffin specimens of yellow ligament from individuals with DM [DM (+)] or non-DM [DM (−)] were stained with rabbit anti-MMP13 antibody followed by Alexa488-conjugated goat anti-rabbit antibody and observed under a confocal microscope. TOTO3 served as a nuclear stain